METALLURGICAL CHARACTERISTICS OF HIGH STRENGTH STRUCTURAL MATERIALS

[Seventh Quarterly Report]

CONTENTS

CONTENTS

ABSTRACT

A progress report covering research studies in high strength structural materials, conducted in the period January 1965 to April 1965, is presented. Fracture toughness index diagrams are presented for titanium and aluminum that define the expected yield strength region of high fracture toughness, requiring plastic overloads for fracture propagation, and low fracture toughness, requiring elastic stresses for fracture propagation, and linear elastic fracture mechanics techniques for determining elastic stress level required for fracture. Results on heat treatment and alloy development studies are reported for several titanium alloys and drop-weight tear test results on some commercially produced aluminum alloys are described. Results of plane strain fracture toughness tests on unalloyed titanium using single-edge-notched and side-notched specimens are reported. Explosion bulge tests on a series of 5Ni-Cr-Mo-V and maraging steel weldments are described in which the results appear encouraging. Low cycle fatigue crack propagation studies on D6AC and 4335 high strength steels are described in which an acceleration of fatigue crack growth rate was seen for each steel in a salt water environment. The 4335 steel test results indicated a stress corrosion cracking condition operating in addition to the action of fatigue cracking.

PROBLEM STATUS

This is a progress report; work is continuing.

AUTHORIZATION

NRL Problem FO1-17; Project SP-00405
NRL Problem MO1-05; Projects SF 020-01-01-0724, RR 007-01-46-5405, and WW-041 (RO5-24A)
NRL Problem MO1-18; Projects SF 020-01-05-0731, RR 007-01-46-5420, WW-041 (RO5-24B) and MIPR Eng-Nav-65-12
NRL Problem MO3-01; Projects SF 020-01-01-0850 and SF 020-01-01-0851

Manuscript submitted July 16, 1965

METALLURGICAL CHARACTERISTICS OF HIGH STRENGTH STRUCTURAL MATERIALS

[Seventh Quarterly Report]

INTRODUCTION

This is the seventh status report covering the U.S. Naval Research Laboratory Metallurgy Division's long-range program of determining the performance characteristics of high strength materials. The program is primarily aimed at determining the fracture toughness characteristics of these materials, using standard and newly-developed laboratory test methods, as well as establishing the significance of the laboratory tests for predicting the service performance of the materials in large complex structures. Although the program is aimed at Navy requirements, the information that is developed is pertinent to all structural uses of these high strength materials. Quenched and tempered (Q&T) steels, maraging steels, titanium alloys, and aluminum alloys are the principal high strength materials currently under investigation.

The fracture toughness index diagrams for titanium and aluminum have recently been modified to indicate the expected yield strength regions of high fracture toughness and low fracture toughness for optimized and nearly optimized materials. The yield strength range of low fracture toughness indicates the region where the linear elastic fracture mechanics approach to fracture toughness determination will be required. The explosion tear test, the drop-weight tear test, and the yield strength relationships, which are the frame-work of the diagrams, indicate the latest test results These include explosion tear and drop-weight tear test results for the 7079, 6061, and 5086 aluminum alloys.

The results of heat-treatment studies on the alloys Ti-6Al-4Zr-2Mo and Ti-6Al-4Zr-2Sn-.5Mo-.5V are described. On the basis of the Charpy V test. these alloys have shown some of the best combinations of strength and toughness. Preliminary data concerning ingot and plate properties of a high purity Ti-7Al-3Cb-2Sn alloy made at NRL are presented. The results of some initial plane strain fracture toughness tests on high interstitial unalloyed titanium

are discussed in which single-edge-notched and side-notched specimens were used. The results indicate that side-notching is helpful in detecting crack instability, but its usefulness beyond that in a practical sense is dependent upon the development of an analytical method for treating the side-notched specimen.

Explosion bulge test results are reported for a series of 5Ni-Cr-Mo-V weldments and for weldments of experimental 12Ni-5Cr-3Mo grade maraging steel. The 5Ni-Cr-Mo-V weldments were made using stick electrodes and were slightly overmatching, 133-136-ksi yield strength (YS) for the plate and 140-145-ksi YS for the weld metal. The general performance of these weldments in the explosion bulge test were good. The results with the 12Ni-5Cr-3Mo maraging steel weldments were also encouraging. In both cases, demonstration of duplication and reproducibility of results using weld wire from large production heats will be required before any fabrication confidence can be established.

Low cycle fatigue crack propagation studies for D6AC and 4335 high strength steels in salt water show a gross acceleration of fatigue crack growth rate at very low strain levels for both steels compared to crack growth rate results obtained in air. A multiplicity of surface cracks formed radially from the fatigue crack front in the 4335 steel specimens tested in salt water. The size and number of these cracks increased with increasing levels of applied total strain range, indicating that for this material the high crack growth rate observed in salt water may be due to the combined action of fatigue cracking and stress corrosion cracking. A comparative summary of the low cycle fatigue performance of some other widely used steels is also presented.

NOTE

A summary report covering the material presented in the seven quarterly progress reports and other pertinent information has been issued separately as NRL Report 6300,

"Review of Concepts and
Status of Procedures for Fracture-Safe Design
of Complex Welded Structures Involving Metals
of Low to Ultra-High Strength Levels".

Copies of this report are being forwarded to the distribution listing of the quarterly report series. The Abstract of NRL Report 6300 is provided below to indicate the coverage of this special summary report

"ABSTRACT

"This report presents integrated analyses and substantiating data on problems of metallurgical optimization and solutions to fracture-safe design and fabrication of large welded structures, utilizing high strength metals. The apparent complexities of attaining practical engineering use of high strength metals derive primarily from lack of appreciation of the close interrelationships that exist between the intrinsic susceptibilities of these metals to various failure modes and the intrinsic structural mechanics features of the structures Metals of high intrinsic resistance to failure must be matched only to structures that are exactly stress analyzable and thereby are restricted to designs of the utmost attainable simplicity and to fabrication by techniques of utmost precision. Such separations are basic to the theme of this report and provide the "starting point" for analyses of the potentials of utilizing various metals, within the range of metallurgically attainable strength levels. The metallurgical problems of optimizing the base metals, welds and heat-affected zones have been complicated by the absence of parametric "frames of reference" required as bases of comparison. The absence of such broad-base guide lines arises from the failure to evolve an adequate understanding of the significance of conventional engineering tests and from the previous absence of definitive tests that provide assessment of failure mode sensitivities across the full spectrum of materials and attainable strength levels. The development of such test procedures has been one of the principal aims of the investigations conducted by the authors and their associates. The spectrum view that has emerged clearly defines metals and specific strength ranges that provide for matching to applications involving conventional fabrication of complex structures as compared to those that require exact design and fabrication. Thus, applications that may provide fracture-safe design based on the use of simple engineering test methods may be separated from applications that require the exact mathematical analyses of fracture mechanics."

TITANIUM ALLOYS

(R.J. Goode, D.G. Howe, and R.W. Huber)

Fracture toughness studies of a spectrum of titanium alloys in the form of 1-in.-thick plates have provided the only reliable means to date of referencing the fracture toughness characteristics of the full spectrum of titanium alloys in thick sections. The reference diagram charts have aided in the development of new alloys and modification of existing alloys, through chemistry and processing, that exhibit improvements in toughness and strength over what was obtainable several years ago. These studies have shown that the behavior of the material in a structural prototype element test, which incorporates a flaw of the acuity normally found in large, complex, fabricated structures, may be predicted from the performance of the material in a simple laboratory test. The structural prototype element, the explosion tear test (ETT), and the laboratory fracture toughness test, the drop-weight tear test (DWTT), for titanium have both been described in earlier reports (1-4). The correlation of the results of these two tests have provided the necessary information for establishing meaningful fracture toughness specifications for titanium alloys that could not otherwise be evaluated validly by fracture mechanics tests.

THE TITANIUM FRACTURE TOUGHNESS INDEX DIAGRAM

The results of the fracture toughness studies of titanium are presented in the fracture toughness index diagram (FTID) in Fig 1. This diagram has been up-dated to present the latest information, however, it is considered preliminary in comparison to that evolved for steels which shows a "break out" of effects of metal processing. The fracture toughness, as measured by the DWTT, was determined in the strong (RW) and weak (WR) directions (5). The optimum materials trend line (OMTL) indicates the highest DWTT energy value obtained as a function of yield strength (YS) and establishes a "yardstick" for 1-in.-thick plate properties in alloy development and processing. The variety of alloys investigated are listed and coded for reference. The large number of points for some of the alloys represents different heats, processing, and heat treatments investigated.

The ETT studies have established the approximate limits of plastic strain required for propagation of fracture in terms of DWTT energy. As shown in Fig. 1, DWTT energy in excess of 1500-1700 ft-lb is required to avoid "flat breaking"

with extensive fracturing or shattering which is characteristic of fracture propagation under elastic loading conditions. DWTT energies of 2000-2500 ft-lb indicate that 1-2% plastic strain is assured in the ETT and 3-5% plastic strain is generally expected. Above 2500-ft-lb DWTT energy, higher plastic strains than the assured 3-5% would be expected. The extension of these ETT performance limits to the OMTL defines the highest level of yield strength that should be metallurgically attainable for each level of plastic strain. For example, 1-2% would be the expected level of plastic strain attainable at approximately 135-ksi YS, while at about 145-ksi YS and above only elastic strains would be required to cause fracture propagation. The fact that the DWTT energy values for many of the alloys are not close to the OMTL is indicative of either poor chemistry, high interstitial level, non-optimized processing or heat treatment, or a combination of these conditions. As stated in previous reports, it is expected that increasing plate thickness will move the OMTL to lower levels of strength. Studies in this area are being initiated on 2-in. and 3-in.-thick plates of several heat-treatable alloys.

The first results of studies on the plane strain fracture toughness (K_{I_C}) are reported elsewhere in this report. However, based upon the analysis developed for steels which is described in detail in Ref. 6, a projection can be made as to the limits to which the fracture mechanics approach should produce valid fracture toughness and flaw size data for 1-inch titanium using center or single-edge-notched fracture mechanics specimens.

The projection of the 1-2% plastic strain limit band at 1500-1700 ft-lb DWTT energy to the OMTL indicates that for "optimized" titanium alloys of 1-in.-thickness the linear elastic analysis criteria of plastic zone size can be maintained on all materials exceeding about 140-ksi YS and that valid K_{I_C} values should be obtainable. Also, alloys above 140-ksi YS should be expected to propagate fractures at elastic load levels and these materials should definitely be analyzed in fracture mechanics terms. On the basis of population density (the "two block" analysis described for steels, titanium, and aluminum in Ref. 6), most materials between 120 and 140-ksi YS should also be expected to propagate fractures at elastic stress levels, unless the material has been metallurgically and process "optimized" to the highest attainable level of toughness.

Below 120-ksi YS, a wide variety of alloys should be expected to require large plastic overload for fracture propagation and should not be analyzable by present fracture mechanics procedures -- i.e., the fracture toughness is too high for valid fracture mechanics test measurement.

HEAT-TREATMENT STUDIES

Heat-treatment studies on a number of titanium alloys have been continued in order to develop information on the stability of the alloys and to determine the heat treatments which will produce an optimum combination of strength and toughness.

The results of solution annealing and aging treatments for the alloys Ti-6Al-4Zr-2Mo (T-55) and Ti-6Al-4Zr-2Sn-.5Mo-.5V (T-68) are shown in Tables 1 and 2 respectively. The treatment includes solution annealing at temperatures below the beta transus for 1 hour in an argon atmosphere followed by air cooling or water quenching. The specimens were aged in most cases at 1100°F or 1200°F for 2 hours in an argon atmosphere and water quenched or air cooled.

The variation of fracture toughness with heat treatment was determined by using the Charpy V (C_v) test. The specimens were tested at -80°F and +32°F in RW and WR orientations. The C_v and tensile (0.313-in.-diam) specimens were prepared from "as-received" material prior to heat treating, and the tensile specimens were tested at a strain rate of 0.002-in./in./min. The standard 0.2% offset was used in determining yield strength.

Figures 2 and 3 show the effects of variations in solution annealing temperatures on the YS of the two alloys with aging treatments. Water quenching after the solution anneal resulted in considerably higher YS values over that developed by air cooling. The highest YS level is obtained by solution annealing just below the beta transus followed by a water quench. In Fig. 3 the YS of T-68 after water quenching at the 1850°F solution anneal tends to vary according to the specimen's location in the heat-treating muffle The thermal profile in the muffle is such that some of the specimens were at or slightly above the beta transus of the alloy. Metallography confirmed that the corresponding decrease in YS was associated with the characteristic rapid grain growth during beta grain formation.

Figures 4 and 5 are summaries of the C_v energy and YS relationships for the alloys Ti-6Al-4Zr-2Mo (T-55) and Ti-6Al-4Zr-2Sn-.5Mo-.5V (T-68). The lines indicate the optimum materials trend line for these materials based on the C_v test. Since the point above these lines at 145-ksi YS for T-68 is outside the normal scatter of data points and has not been confirmed by additional testing, it was not considered in establishing the optimum line even though it may be valid.

Figure 6 shows the effect of selected heat treatments on the C_v energy of the alloys Ti-6Al-4Zr-2Mo (T-55) and Ti-6Al-4Zr-2Sn-.5Mo-.5V (T-68) in the 120-140-ksi YS range. The values illustrated and the heat treatments were taken from Tables 1 and 2 and represent the nearest approach to an optimum condition for the alloys.

Table 3 shows the strength of tensile specimens taken from heat-treated drop-weight tear test (DWTT) pieces of the alloy Ti-6Al-2Mo (T-22). For comparison, the results of tensile strengths previously reported for this alloy (7) on specimens machined before heat treatment are included. As might be expected, the data show the pre-machined (small-size) specimens have somewhat higher strengths than those taken from the 1-in.-thick heat-treated DWTT pieces. Sufficient material was not available to obtain tensile specimens in the longitudinal direction of the DWTT piece that was heat treated at 1750°F for 1 hr in an argon atmosphere and air cooled. The aging treatment for this piece consisted of 1100°F for 2 hrs in an argon atmosphere followed by water quenching. Previous work has shown the tensile strengths are generally 3,000-4,000-psi higher in the longitudinal direction for this particular material and one could assume that the YS of this DWTT piece in the longitudinal direction would be greater than the 118,800-psi YS in the transverse direction, or approximately 122,000-psi.

Of all the alloys investigated to date in the heat-treating studies, the alloys Ti-8Al-1Mo-1V (T-19), Ti-6Al-4Sn-1V (T-20), Ti-6Al-2Mo (T-22), Ti-6Al-4Zr-2Mo (T-55), and Ti-6Al-4Zr-2Sn-.5Mo-.5V (T-68) have shown the best combinations of strength and toughness. Figure 7 shows the summary of C_v energy and YS relationships of these alloys. The curves indicate the OMTL for the respective alloys. However, the weld and heat-affected-zone (HAZ) properties of some of these alloys may be difficult to optimize both as to strength and fracture toughness.

ALLOY DEVELOPMENT STUDIES

A promising combination of strength and toughness properties was reported for a Ti-7Al-2Cb-1Ta-2.5Sn alloy by IIT Research Institute (8). Based on these findings, a high purity, low interstitial (approximately 0.04 oxygen) Ti-7Al-3Cb-2Sn alloy (T-76) was made using the consumable electrode vacuum arc remelting technique. The metal was vacuum cast into a 4-in. x 7-in. x length copper chill mold after melting in the NRL skull melting furnace. The as-cast DWTT energy for a 1-in. section removed from this billet was 2808 ft-lb. Half of the remaining billet was forged to a 1-1/4-in. slab and hot-rolled at 1650°F into a 1-in.-thick plate. A portion of this plate was solution annealed at 1925°F for 1/2-hr, air cooled, then aged 2 hrs at 1100°F. The resultant properties after heat treatment were DWTT energy - 1723 ft-lb, 117-ksi UTS, 109-ksi YS, 9% RA, and 17% Elong. Additional studies on this alloy are in progress.

Two $\alpha+\beta$ titanium alloys - designed for the 130-150-ksi YS range - were double vacuum arc melted into 9-in.-diam, 120-lb ingots. These ingots are being forged into billets at a commercial production facility at 2100°F and the billets are then to be hot-rolled at 1750°F for 1-in. plate.

ELECTRON BEAM WELDING

The new laboratory facilities for conducting experimental and developmental studies on electron beam welding techniques and procedures for titanium became available in February 1965. A new 60-kv to 30 kw electron beam welder with a 30-in. x 50-in. x 42-in. chamber has been installed. Voltage, power inputs, and travel speed parameters are being established for a variety of titanium, steel, and aluminum alloy plates in various thicknesses. Simulated plate welds through 2-1/2-in. titanium have been made at 40-in./min. travel, and the depth-to-width ratio is greater than 15 to 1. The fracture toughness properties of electron beam welds in titanium alloys will be studied and compared to the inert gas MIG type of welds.

EXPLOSION BULGE TESTS OF 5Ni-Cr-Mo-V WELDMENTS

(P.P. Puzak and K.B. Lloyd)

The previous (sixth) progress report (9) presented a general review of the extensive data provided by the United States Steel Corporation's development program under the Bureau of Ships HY 130/150-ksi yield strength (YS) hull steel contract. The particular 5Ni-Cr-Mo-V alloy system developed in this program was designed to provide a steel with secondary hardening characteristics such that with a given carbon content, the YS developed by quenched and tempered (Q&T) heat treatment would essentially be the same for tempering treatments in the range of 900° to 1100°F. Several large-size (80-ton) production heats of the 5Ni-Cr-Mo-V steel have been produced, and test data have shown the plate material to exhibit relatively high fracture toughness for YS levels within the HY 130/150-ksi range. It should be noted that the C_v properties reported by the United States Steel Corporation for 1-in. and 2-in. plates of early production heats were checked by NRL and found to be in close agreement. By relatively minor chemical composition and heat-treatment (tempering temperatures) adjustments, it should be possible to produce high fracture toughness plates of this alloy composition to YS levels ranging from approximately 130 to 150-ksi for thicknesses of 2-in. to 4-in., or for possibly somewhat higher thicknesses.

The development of reliable filler metals for joining high strength Q&T steels is a much more difficult metallurgical problem than is the case for the base plate. For large complex structures, the weld metal strength and toughness must be maintained without requiring full Q&T heat treatment after fabrication, and the weld must be crack-free. The welding parameters (low preheat and energy input) which are favorable for the development of high weld-metal strengths are invariably found to increase cracking sensitivity and decrease toughness. A summary of C_v and YS relationships that have been reported by USS-Airco (10) for experimental welds is given in Fig. 8 for manual (covered) electrodes and in Fig. 9 for semiautomatic, inert gas shielded (MIG) welds. The shaded areas in Fig. 9 represent the data band shown in Fig. 8 for the covered electrodes. It can be seen that the development of MIG weld metals has substantially progressed to a point where welds with yield strengths of 130 to 140-ksi and C_v values of approximately 100 ft-lb at 30°F can be

can be produced under laboratory conditions. The covered electrode welds are characterized by considerably lower C_v values with a maximum value at 30°F of 45 ft-lb for the best of the HY 140-ksi covered electrodes available at this stage of development.

The previous progress report (9) had also presented the results of explosion bulge testing of three of the 5Ni-Cr-Mo-V 1-in. steel plates welded with 140-ksi YS MIG weld metal in the downhand, or horizontal, position. The plate metal yield strengths had been varied from 130 to 150-ksi to permit investigation of the relative performance of undermatching, matching, or overmatching weldments. Weld metals with yield strengths overmatching that of the new alloy base plate (such as is presently employed for HY-80 hulls) would require approximately 160-ksi minimum YS to overmatch the 150-ksi capabilities of the 5Ni-Cr-Mo-V plate material. On the premise that suitably tough HY 140 (but not HY 150 minimum) weld metals were available, or could be developed within the time-frame of the USS-BuShips contract for an HY 130-150-ksi hull weldment, a weldment evaluation program aimed at providing a guaranteed HY 130-ksi minimum YS weldment has been initiated. Explosion bulge tests have now been conducted for additional samples of a new production heat of 5Ni-Cr-Mo-V steel plate heat treated to the low end of the strength level range and welded manually with the best of covered electrodes and MIG weld metals developed to date under the USS-BuShips contract.

The current series of explosion bulge tests were conducted on plate specimens assembled by four sub-contractors to the United States Steel Corporation: Airco, Arcos, Linde, and McKay, each using the new weld metal evolved by the various companies for this application. The welding with covered electrodes produced by Airco, Arcos, and McKay from small laboratory heats of core wire had been performed in the flat, or downhand, position. Other specimens had been manually welded by Airco and Linde with a MIG, interrupted-arc, out-of-position (vertical-up) welding technique. The MIG filler wires comprised material from a large (17-ton) air melt production heat for the Airco weldments and a small (1/2-ton) vacuum melt heat for the Linde weldments. Each company had submitted a set of three 1-in -thick, single V-joint preparation weldments made with their respective weld metals. One of each set was ground smooth, removing the weld crown, and gridded for field (test-site) measurement of surface strain and thickness.

A second weldment of each company was tested "as-welded" with the weld crown, or reinforcement, intact. The third weldment of the set was modified at NRL by the addition of a crack-starter weld in order to develop preliminary information concerning the performance of these materials in the presence of cracks. An extra MIG, interrupted-arc weldment was supplied by Airco and was tested with the weld crown intact.

A summary of the mechanical properties data determined by the United States Steel Corporation for the plates and new weld metals used for the current explosion bulge specimens is given in Table 4. Plate metal properties were determined with specimens cut from test coupons that were heat treated simultaneously with the plates that were subsequently welded by the various sub-contractors. Weld metal properties were determined with specimens cut from an extended length of one of the bulge test weldments prepared by each sub-contractor. Generally, the results in Table 4 indicate that overmatching welds were produced in all cases, and that plate metal toughness (as shown by C_v tests) is considerably higher than that of any of the five weld metals under evaluation. The MIG weld metal toughness (as shown by C_v tests) are noted to be considerably higher than that of the covered electrode weld metals. The Linde MIG weld metal which has the highest C_v value at 30°F is also noted to be the lowest in YS (135-ksi) of the various weld metals.

The crack-starter modified weldments were tested first. Each specimen received two 7-lb Pentolite explosive charge shots, at 15-in. stand-off distance and at 30°F test temperature. The crack-starter weld on the weld crown intentionally introduces an early flaw into the test area and provides for quick screening of samples that have tendencies for catastrophic propagation of the crack in weld, heat-affected-zone (HAZ), or fusion line. The development (or extension), after one or two shots, of fractures which extend into or through the hold-down regions of the crack-starter modified samples is indicative of low toughness and considered to be below acceptability levels.

Figures 10 and 11 present the appearance of the crack-starter modified weldments after completion of the tests. The first shot had produced relatively short fractures in each specimen: the second shot extended these cracks as

illustrated. In general, the crack-starter test results shown in Figs. 10 and 11 are encouraging when one considers the relatively high strengths of the plate and weld metals. Plate metal fractures and HAZ tearing are confined well within the plastically deformed, bulge, region of the samples. Dominant crack propagation in weld metal is apparent only in the Arcos (covered electrode) weldment, which is also characterized, Table 4, by the lowest C_v values (33 ft-lb) of the various weld metals being investigated.

As described above, crack-starter modified bulge tests are terminated after completion of two shots. Conventional bulge test procedures, however, require repetitive testing of the weldment by repeating the cycle of refrigeration, firing, and examination until failure occurs, or until the development - without visible failure - of a limiting bulge depth (bulge limit established by BuShips for the service application involved). Bulge testing experience has shown that a secondary apex-bulge (equivalent to localized necking) can be expected to develop in 1-in.-thick samples after the development of approximately 15 to 18% thickness reduction of the plate. Continued testing is not warranted for weldments that develop secondary bulge conditions without visible failure.

Pertinent details of the explosion bulge tests of the as-welded (weld crown intact) samples are summarized in Table 5. Figures 12 and 13 illustrate the appearance of these samples after completion of the tests. Visible fractures were not developed until after six shots in two of the covered electrode weldments (McKay and Arcos) and in one of the MIG interrupted-arc, vertical-up weldments. In general, these fractures were relatively short and no signs of brittleness were apparent. Additional testing of these samples had been discontinued because of visible evidence of secondary bulging and comparatively high (17 to 19%) thickness reduction in the plate following the sixth shot, Table 5. Relatively high toughness characteristics are also indicated by results obtained with the Airco covered electrode weldments and both of the MIG interrupted-arc weldments. The weld metal and toe cracks which developed after the fourth shot on the Airco covered electrode weldment were extended only slightly by the application of the fifth shot. Similarly, the crack indications which developed after two shots on the MIG weldments were extended only slightly by two additional test

shots. The initial visible evidence of fractures in these weldments may be related to inherent weld metal defects and the stress concentration at the toe of the weld crown.

The weld crown on one weldment of each set was ground smooth and a scribed grid on each was used to provide precise points at which thickness reduction and surface strain measurements could be made. The curves derived from the thickness reduction measurements made after each shot in the covered electrode weldments are shown in Fig. 14. Generally, similar data were obtained for the MIG interrupted-arc weldments. The weld metal thickness reduction is noted to be slightly less than that of the adjacent plate metal, and an approximately uniform reduction in thickness is developed by each successive shot excepting the final shot applied to the Airco weldment. It is apparent that the much larger thickness reduction developed by the sixth shot on this plate is limited to the apex of the bulge and this is considered to be indicative of secondary bulging.

The appearance of the ground-smooth samples of covered electrode weldments after completion of the bulge tests is shown in Fig. 15. A weld metal flaw in the McKay weldment that was not detected by radiographic or visual inspection prior to testing resulted in development of a short, V-shaped tear across the width of the weld on the first shot. Application of a second shot resulted in moderate extension of the initial crack into the base plate as illustrated in Fig. 15. Longitudinal cracks developed on the sixth shot at the edge of the welds, indicated by the arrows, on the other two smooth-ground weldments. Additional shots were not applied to these samples because they had developed a full-bulge and visual indications of secondary apex-bulge characteristics.

Bulge test conditions are generally less severe for weldments that are ground smooth than is the case for weldments with the weld crown intact. The stress concentration at the toe of the weld crown tends to promote the development of HAZ or fusion line cracks which propagate extensively in cases where brittle paths of fracture exist. This condition has not been evident in any of the previously illustrated weldments of the 5Ni-Cr-Mo-V steel that were shown to develop longitudinal cracks at the toe of the weld crown. The ground-smooth Airco and Linde MIG interrupted-arc weldments, however, developed longitudinal, through-the-plate ruptures after four and six shots respectively, as shown in Fig. 16. In both of these samples, the longitudinal

ruptures appear to have propagated predominantly in the fusion line of these single V-joint preparation weldments. Both of these weldments had sustained extensive bulging and thickness reduction of the plate prior to developing the illustrated ruptures and additional testing was not warranted. Metallographic examination of these and other samples (being conducted by United States Steel Corporation personnel) and additional bulge tests are required to establish whether, in fact, a preferential path of fracture is developed in weldments fabricated by the MIG interrupted-arc (vertical-up) welding technique.

Explosion bulge tests conducted to date for 5Ni-Cr-Mo-V alloy steel weldments have involved five different weld metals (two MIG and three covered electrodes) as well as three welding procedures. The welding procedures were manual stick, manual MIG interrupted-arc (vertical-up), and automatic MIG. These tests are considered of exploratory nature. It should be recognized that BuShips qualification requires demonstration of performance with six or more 2-in.-thick weldments of a given material (or procedure) to be tested with weld crown intact. Explosion bulge tests conducted to date have involved only 1-in.-thick weldments and a very limited number of samples of a given material. Results in general have been encouraging and the following tentative conclusions pertaining to the 1-in.-thick tests reported herein appear to be warranted:

1. At a yield strength of 130 to 135-ksi, the 5Ni-Cr-Mo-V plate material exhibits high fracture toughness as is evident by relatively short tears confined to the plastically deformed regions of the crack-starter and bulge test plates. Further confirmation of the fracture toughness of this steel has been provided by drop-weight tear tests (DWTT) of another 1-in. steel plate (134-ksi YS) from the same heat of steel used for this weldment evaluation program - the DWTT energy for this plate was over 5000 ft-lb.

2. There appears to be no evidence in any of the 1-in.-thick explosion bulge specimens tested to date of low HAZ fracture toughness resulting from welding on this 5Ni-Cr-Mo-V steel plate.

3. The initial exploratory test results with overmatching welds are encouraging, however, additional tests to determine suitability and reproducibility with production lots of electrodes are required to establish fabrication confidence.

EXPLOSION BULGE TESTS OF EXPERIMENTAL MARAGING STEEL WELDMENTS

[P.P. Puzak and K.B. Lloyd]

Among the new materials of interest for use in large welded structures are the new maraging steels. These comprise a variety of new steel compositions which are capable of developing high strength levels by annealing and aging treatments. The 12%Ni-5%Cr-3%Mo grades represent a comparatively recent development of this family of steels. Depending upon heat treatment and combined content levels of the hardening elements (Al and Ti), the 12-5-3 maraging steels exhibit yield strengths ranging from 150 to 215-ksi. Fracture toughness evaluations previously reported(2) for seven experimental small (1/2 and 1-ton) mill heats of the 12-5-3 maraging alloys rolled to 1-in. plate indicated considerably higher fracture toughness properties than the 18%Ni-8%Co-3-5%Mo maraging alloys that are capable of developing yield strengths in the range of 200-300-ksi. Plates of 1-in. to 2-in.-thickness of 180-ksi minimum yield strength (YS) and high fracture toughness properties (in excess of 50 ft-lb C_v at 30°F) can be produced with the 12Ni-5Cr-3Mo maraging steels.

The primary potential advantage of these new 12-5-3 maraging steels lies in the possibilities that are provided for welding fabrication of fracture tough 160-180-ksi YS materials. In order to develop such fabrication capabilities for the best of the conventional quenched and tempered (Q&T) steels, it is presently necessary to apply a full-cycle, Q&T, heat treatment to the weldment. Without such full-cycle heat treatment, the best of the available welds (not necessarily the plates) for Q&T steels are brittle. Weldments of the maraging steels also require a post-weld heat treatment to develop strength and toughness in the weld metal and heat-affected-zone (HAZ). However, as contrasted with the full-cycle, Q&T, heat treatment, the aging treatment at approximately 900°F for maraging steels is comparatively simple compared to the Q&T type heat treatments. For relatively small structures of simple design, conventional furnaces could be employed for maraging of the whole structure without concern for excessive shrinkage or sagging of the structure as would be the case for the full-cycle, Q&T, heat treatment. For large structures, it may be feasible to accomplish maraging by local heating of the weld joint area.

The initial development studies for weld metals necessary to fabricate the new 12-5-3 maraging steels did not fully succeed in matching plate metal properties. Weld deposits similar in alloy composition to those of the plates were found to develop properties (after aging) of lower strength (approximately 160-ksi YS) and toughness (approximately 40 ft-lb C_v at 30°F) than those of the 180-ksi YS plates. Continuing research efforts were aimed at developing fracture tough weld metals that equaled the YS and toughness of the 180-ksi minimum YS base plate to provide weldments with 100% joint efficiency. Recent weld metal developments by the International Nickel Company (INCO) revealed that certain filler wire compositions of the 18-8-3 type (not disclosed) were compatible with the 12Ni-Cr-Mo maraging steel plate. With the new filler wire, weld metal properties (after aging) were stated to be approximately equivalent to those of the 12-5-3 plate at 180-ksi minimum YS. A cooperative investigation involving a limited number of explosion bulge tests was undertaken to assess the weldment performance of these welds in a 180-ksi YS maraging steel.

To expedite preparation of the bulge test samples, it was necessary to use weld wire produced by vycor-extraction techniques from several small laboratory heats of the new alloy. The wire was prepared and used by INCO Research Laboratory personnel to TIG (tungsten inert gas) weld 1-in.-thick plates (NRL #H-7) rolled from an air melt heat of the 180-ksi YS grade of the 12-5-3 maraging steel. The sample was furnace-aged after welding and tested by NRL. After completion of the bulge test, chemical analysis of the weld deposit revealed the combined average composition of the hardening elements (Ti and Al) to be below the desired aim level necessary to insure the development of 180-ksi YS in the weld deposit. Plates (NRL #H-8) rolled from a CEVM (consumable-electrode-vacuum melt) heat of the 12-5-3 maraging steel were used for a second weldment. Although similar techniques were employed to produce the TIG weld wire, the laboratory melts were adjusted in composition to compensate for the anticipated loss in Ti and Al contents during vycor-extraction.

Property data jointly established by the cooperating laboratories for plate and weld metal in the maraging steel bulge test specimens are summarized in Table 6. It should be noted that tension test results with specimens oriented transverse to the weld may not be fully

representative of weld metal values that might be obtained with all weld metal tension specimens. However, analysis of the data given in Table 6 indicates the weld of the first bulge test specimen to be an undermatching (i.e., weld metal YS lower than plate metal YS) weldment. Confirmation of an undermatching weldment condition is provided by the tension test specimen failure in the weld metal and the significantly lower weld metal hardness values (34/36 R_C) compared to those (43/44 R_C) of the plate in the first maraging steel bulge test specimen. From a similar analysis of the data for the second bulge test specimen, the 176-ksi YS indicated in Table 6 (with tension specimen failure in the HAZ) is considered to be lower than the true value for the second weld metal (#WMA-2). The weld metal hardness values (42/43 R_C) were slightly higher than those of the plate (41/42 R_C). It is estimated that an equal or slightly overmatching weld was produced with the YS of the weld being slightly higher than the 179-ksi measured for the plated.

The explosion bulge tests were conducted at 30°F using 7-lb Pentolite charges and 15-in. standoff. Past explosion bulge test experience has indicated that, if the weld crown is not ground smooth, the strain concentration at the toe of undermatching welds tends to promote complete separation of the bulge test specimens on the first or second shot. Both of the maraging steel bulge test specimens were tested with the weld crown intact. The bulge test performance of the undermatching weldment was similar to that of other undermatching welds; after the first shot, a 1-1/4-in.-long tear was visible at the toe of the weld crown, Fig. 17, top. The depth of bulge was approximately 1-inch, Fig. 17, bottom, and a surface strain of approximately 2% in the plate metal adjacent to the weld was measured after the first shot. A second shot resulted in complete separation of this bulge test specimen as shown in Fig. 18.

Similar test conditions to those described above were employed for the second maraging steel weldment. Following the second shot, two small toe-cracks, each approximately 2-in.-long, were visible at the apex of the bulge along the toe of the weld crown. A 1-1/2-in.-bulge depth, 3-1/2% weld metal surface strain, and 4-1/2% surface strain in the plate metal adjacent to the weld, were measured after the second shot. Application of a third shot to this specimen resulted in only short extensions of the original toe-cracks, Fig. 19. Normal bulge test procedures

would have resulted in termination of this test after the third shot, but observing the short extensions and apparently shallow depth of the toe-cracks after the third shot, it was decided to apply a fourth shot to this specimen. Following this shot, the weldment toe-cracks were extended to 4-1/2 to 5-in. in length, and several short (1/4-in.) cracks in the weld metal were visible at weld-ripple positions, Fig. 20, top. None of the cracks had penetrated through the thickness of the weldment and a bulge depth of 2-5/8-in. was measured, Fig. 20, bottom. Further testing of this weldment was discontinued to permit cutting of test specimen blanks from non-deformed hold-down regions of the bulge sample.

The specific maraging heat treatments applied to the bulge test specimens were based upon exploratory laboratory (INCO) results of tension and Charpy V (C_v) tests of the different plate and weld materials. The specimens removed from the hold-down regions of the bulge test samples reflect the properties developed by the respective aging heat treatments noted in Table 6. In addition, C_v and tension test results were obtained for the two plate materials in the conventional maraging condition (3 hours at 900°F). A comparison of these data with those of other 1-in.-thick steels is provided by illustrating the C_v values of the maraging steel plates and weld metals as a function of the yield strengths of the test materials, Fig. 21. The curves in this illustration depict the OMTL (optimum materials trend line) for characteristic groups relating to processing variables (melting practice and/or crossrolling) of the steels studied to date (9). From the data shown in Fig. 21, it is apparent that both the air melt (#H-7) and CEVM (#H-8) plates developed yield strengths in excess of 180-ksi when aged for 3 hours at 900°F. For this aging treatment, the C_v values exceed 50 ft-lb for the CEVM plate and 40 ft-lb for the air melt plate. The C_v values of 50 and 41 ft-lb illustrated for the new filler wires are considered promising in view of the relatively high yield strengths (approximately 167 and 180-ksi respectively) for the weld metals involved.

On a single test basis of experimental materials, it is not warranted to draw general conclusions. However, explosion bulge test results for the second sample with a non-matching alloy filler wire in the new 12Ni-Cr-Mo, 180-ksi YS grade of maraging steel may be considered promising. Comparatively high toughness was demonstrated

by this 1-in.-thick plate weldment which showed the capability of developing additional local plastic deformation with only small extensions of the toe-line cracks formed during the previous explosion tests of the bulge sample. It should also be recognized that the weld wires used in this exploratory investigation of maraging steel weldments comprised material from small experimental laboratory heats. More extensive evaluations of the potentials of the 12-5-3 maraging steels for high strength weldment fabrication are planned for future investigations. It must still be demonstrated that similar results can be duplicated or exceeded with weld wires produced from large-scale production heats before further conclusions can be drawn concerning the suitability of using the new alloy filler wire in the welding of 12-5-3 maraging steel plates for general applications in welded structures.

LOW CYCLE FATIGUE CRACK PROPAGATION IN D6AC AND 4335 HIGH STRENGTH STRUCTURAL STEELS

[T.W. Crooker, R.E. Morey, and E.A. Lange]

The safe and dependable application of modern high strength materials to large cyclically loaded structures, such as pressure vessels and submersible vehicles, requires an improved knowledge of slow crack propagation from low cycle fatigue. Small flaws and cracks invariably are formed during fabrication and manufacture of a large welded structure, despite the use of the best available processing and inspection techniques. Since fabrication flaws are unavoidable, the only practical recourse is to provide design criteria for preventing the growth of such cracks to a critical size from repeated service loads.

The aim of this investigation is to define and evaluate the factors which control the growth of cracks under low cycle fatigue conditions. The results of the current phase of this investigation are based on studies of crack propagation in center-notched plate bend specimens loaded in cantilever fashion. Preliminary evaluations of the low cycle fatigue characteristics of a wide variety of materials including normalized and quenched and tempered (Q&T) steels, Ni-Cu Monel alloys, a 2024 aluminum alloy, and titanium alloys, have been made (2,7,9,11-15). Briefly, it has been observed that for a specific environment and strain ratio, the growth rate of a low cycle

fatigue crack is dependent upon applied total (elastic plus plastic) strain range, as expressed by the relationship $dL/dN = C(\varepsilon_T)^m$ where L = total crack length, N = cycles of loading, ε_T = total strain range, m = exponent, and C = constant.

This relationship remains valid in the presence of mean strains other than zero and in the presence of aqueous corrosive environments for most materials. However, it has been observed that both of these factors affect crack growth rate. Mean strain can either accelerate or retard crack growth rate, depending upon whether it is tensile or compressive. Corrosive environments tend to accelerate crack growth rate, depending upon such factors as corrosion resistance, stress corrosion cracking, and hydrogen embrittlement.

MATERIALS AND PROCEDURE

The materials tested for this report are two conventional high strength steels, D6Ac (code G85) and 4335 (code G98). Chemical compositions and tensile properties of these materials are shown in Tables 7 and 8.

Specimens of both materials were finish machined before they were given the following heat treatment. For D6AC steel specimens: the material was austenitized in a hydrogen atmosphere for 1 hour at 1625°F, quenched in oil for 15 minutes at 400°F, and then cooled in air. Tempering was 1 hour at 400°F followed by air cooling. Specimens were then double tempered at 1025°F for 2 hours and air cooled after each temper period. For 4335 steel specimens: the material was austenitized in a hydrogen atmosphere for 1 hour at 1625°F, followed by quenching to below 100°F in oil. A double temper of 2+2 hours at 600°F was given with an air cool following each temper period.

The two materials, D6AC and 4335, were chosen for study because of their wide application as high strength materials for structures having highly refined designs. Knowledge of the growth rate of fatigue cracks in these materials is important to the safe application of these materials to other, less highly refined, structures; since these materials permit the propagation of fast fractures through elastically loaded regions from small flaws.

The experimental procedure employed for this series of tests is the same as that described in the references.

Experimental data are based on the observed macroscopic growth of fatigue cracks across the surface of center-notched plate bend specimens. These specimens are cantilever loaded under full-reverse cycling in both air and 3.5% salt water environments. Constant total strain range loading conditions are maintained by adjusting deflection, and the corresponding crack growth rate is measured. Nominal surface strains are measured with electrical resistance strain gages. The strain range-deflection characteristics of these materials in the plate bend specimens are shown in Fig. 22.

Each specimen is successively tested at a specific total strain range value for an interval of several hundred to several thousand cycles, until the crack growth rate can be established accurately, and then this procedure is repeated at a higher strain level. With this procedure, a series of crack growth rate versus total strain range data points are obtained from each specimen. For tests conducted under a salt water environment, a corrosion cell is positioned on the specimen, allowing the salt water solution to flow over the fatigue crack from a reservoir during testing.

STRAIN RANGE EFFECTS

Fatigue crack growth rate versus applied total strain range data for D6AC and 4335 steels in an air environment are shown plotted on a log-log scale in Fig. 23. These two materials were heat treated to essentially the same yield strength (YS) levels, and therefore they exhibited nearly identical proportional limits in the plate bend specimen. The total strain range (tension plus compression) at the proportional limits was 16,000 microinches/inch as indicated on Fig. 23. The basic resistance of a material to the growth of fatigue cracks is most visible on a strain range basis, and this will be discussed first. The comparison of a variety of materials for structural applications is more appropriately conducted relative to YS or, in our case, the proportional limit.

Low cycle fatigue crack propagation in these two materials is characterized by high sensitivity to applied strain, as indicated by the steep slope of the curves, Fig. 23, and the development of very rapid crack growth rates (i.e., $\frac{dL}{dN} > 1000 \frac{\text{microinches}}{\text{cycle}}$) under elastic loading.

Unlike previous materials tested, crack growth rates in these two materials over the range of strain values examined do not follow a single exponential relationship with respect to applied total strain range. Instead, the relationships assume a steeper slope above applied strain values near 50% of the proportional limit. This phenomena of increasing sensitivity to applied strain at high elastic strain levels has been observed in high strength steels by other investigators (14) and is yet to be fully explained.

It should be reported that fast fracture was not initiated in the plate bend specimens of either steel even with surface crack lengths of 1.3-in. and tensile strains of 6,800 microinches/inch corresponding to a stress level of 204,000 psi.

WET FATIGUE

D6AC and 4335 steel fatigue specimens were also tested in a 3.5% salt water environment. The results of these tests are shown on a log-log plot of fatigue crack growth rate versus applied total strain range in Fig. 24. The plots of similar data taken in air are shown in dashed lines for comparison.

As might be expected, the introduction of a salt water environment results in a gross acceleration of fatigue crack growth rates (i.e., more than an order of magnitude), even at very low strain levels below 25% of the proportional limit. However, a comparison of the two curves reveals that these two steels did not react to the aqueous environment in the same manner. Although 4335 exhibited slightly more crack propagation resistance than D6AC in air, as indicated by the locus of its data points falling to the right of D6AC, it was more severely affected by the salt water environment. During testing under salt water, the 4335 steel was observed to form a multitude of surface cracks which propagated radially from the fatigue crack front. The size and number of these cracks increased with increasing levels of applied total strain range. The existence of these cracks strongly suggests the possibility that the very rapid crack growth measured in 4335 steel under salt water occurred as a result of the simultaneous action of fatigue cracking and stress corrosion cracking.

The D6AC steel did not exhibit such secondary surface cracks. Nevertheless, its fatigue performance was severely affected by the presence of the salt water environment. Since Q&T steels of this YS level are suspect of cracking in even "pure" water environments (15), these results are not surprising. However, when compared with the wet fatigue performance of lower YS materials (7,9,12,13), these data serve to point out the very difficult problems which can exist in the application of D6AC and 4335 steels in a water environment at design stresses demanded of high performance structures.

COMPARATIVE FATIGUE PERFORMANCE

A comparative summary of the low cycle fatigue performance of six popular structural steels is given in Fig. 25. This log-log plot shows the fatigue crack growth rate versus the ratio of applied total strain range to proportional limit strain range for each material in an air environment. The materials plotted are as follows: A201B (48-ksi YS), HY-80 (88-ksi YS), T-1 (107-ksi YS), Q&T 150 (HY-80 composition)(157-ksi YS), 4335 (215-ksi YS), and D6AC (212-ksi YS).

Fig. 25 clearly illustrates several important points which are fundamental and must be considered in the application of high strength steels to large cyclically-loaded structures. First, it is apparent that resistance to slow fatigue crack growth under localized plastic strain conditions decreases rapidly with increasing yield strength. As YS levels exceed 150-ksi, fatigue crack growth rates increase rapidly, at nominal elastic strain levels below the proportional limits which are normally considered for design criteria.

In addition, the sensitivity of crack growth rates to changes in applied strain levels, such as might be experienced by accidental overloads, increases with YS. Fatigue crack growth rates in low strength pearlitic, carbon steel, A201B, have been found to be proportional to the third power of total strain range; whereas crack growth rates in D6AC loaded to 50% of the proportional limit or higher increase as a function of the sixth power of the total strain range.

These points are summarized in Figs. 26 and 27. In Fig. 26, the fatigue crack growth rate at the proportional limit strain range is plotted against YS. This plot illustrates

the fact that as yield strengths are raised beyond 150-ksi, the problem of fatigue crack growth at high elastic strains involves a new order of magnitude in structural design difficulty.

For designs based on the low cycle fatigue range (i.e., less than 100,000 cycles), nominal stresses will be high and the major portion of the life of the structure will be dependent upon the first small extension of a flaw where the growth does not significantly affect the local strain pattern. After the flaw has grown sufficiently to influence the local strain level, crack growth rapidly accelerates and life is soon terminated. This effect is readily apparent in fatigue tests conducted on a constant load basis. Unfortunately, most laboratory fatigue tests conducted at constant load do not include the effect of flaws and the life observed is predominantly that for crack initiation and the crack growth period is minimal.

For the case of large structures where small flaws are expected and a safe life period depends upon slow extension of a crack by fatigue, knowledge of the relative performance of various materials on a YS basis is very useful. Such comparisons can be made from the relationship shown in Fig. 27, where the allowable relative loading for various steels can be compared for a low life or a high life.

Because crack growth rates correlate well with total strain and strains may extend into the plastic region, the relative load variable in Fig. 27 is expressed as percentage of proportional limit strain range. It turns out that the lateral restrain condition in the plate bend specimen provides the conditions where the proportional limit strain corresponds essentially to the YS of high strength metals as determined in the conventional axially-loaded, smooth, cylindrical specimen. If one is more accustomed to thinking in terms of stress rather than strain, the ordinate in Fig. 27 may be considered as"allowable percentage of yield strength".

An important observation from the 10 KC fatigue life curves in Fig. 27 is that they approach each other with increasing YS. Thus for high strength metals, only a small increase in relative stress level can decrease fatigue life from a high level to a low level which emphasizes the conclusion that consideration of designing for finite life using high strength materials requires

an exact knowledge of stresses and precise control of the loading conditions in service. In fact, above 200-ksi YS, there does not appear to be a prudent safe life period in the low cycle range for large complex structures (involving regions of complex geometry) where life depends upon the slow growth of fatigue cracks. In fact, at YS levels of 150-ksi, careful engineering judgment is required if finite lives between 10,000 cycles and 100,000 cycles are to be considered for large structures. Although the comparison of the fatigue characteristics of materials in Fig. 27 does not include many important considerations concerning stress state and environment, it does provide the "caution light" when increasing structural performance is projected simply by substituting a material with a higher YS and maintaining, or even, as is frequently the case, increasing the nominal relative design stress. The relationships in Fig. 27 readily show why low cycle fatigue was not a problem with old, conventional carbon steels, but they also show that low cycle fatigue becomes a rapidly increasing problem with the use of high strength materials.

CONCLUSIONS

1. The D6AC and 4335 steels tested at a 210-ksi YS level were found to possess significantly lower resistance to low cycle fatigue crack growth in an air environment compared to that for lower strength steels. These high strength steels were found to develop rapid fatigue cracking under nominal elastic loading, and exhibit extremely rapid fatigue crack propagation rates at positions of localized plastic strain.

2. The introduction of a 3.5% salt water environment grossly accelerates crack growth rates in both steels. The 4335 steel was affected to a greater extent and showed visible evidence of extensive stress corrosion cracking.

3. In comparing the low cycle fatigue crack propagation characteristics of structural steels possessing YS levels from 50 to 210-ksi, it is concluded that the problem of low cycle fatigue life in materials such as D6AC and 4335 at a 210-ksi YS level greatly exceeds the design problem of the currently-used lower strength materials for application in large welded structures.

ALUMINUM ALLOYS

[R.W. Judy, Jr., and R.J. Goode]

The fracture toughness studies on the spectrum of aluminum alloys were initiated at a later date than those for steels and titanium. To date, a very preliminary fracture toughness index diagram (FTID) for aluminum has been developed, based on drop-weight tear test (DWTT), explosion tear test (ETT), and yield strength (YS) correlations. This diagram, which has been modified to show new data, is shown in Fig. 28 along with the alloys and tempers studied (indicated next to the data points).

FRACTURE TOUGHNESS INDEX DIAGRAM

The fracture toughness properties of the various alloys as measured by the DWTT were determined in the strong (RW) and weak (WR) orientations (5) and, as indicated by the data points, considerable anisotropy is noted for all but the highest strength alloys. The optimum materials trend line (OMTL) is shown for the strong direction and indicates the highest level of attainable fracture toughness for any given level of strength. The ETT performance correlation with DWTT energy delineates plastic overload capabilities for materials exceeding 200-300 ft-lb DWTT energy. Materials having DWTT energies below 200-300 ft-lb develop and propagate fast-running fractures through elastic stress fields; this is characterized in the ETT by generally flat breaking, accompanied with either extensive fracturing or shattering. Above 300 ft-lb DWTT energy, plastic overload capability of the material is demonstrated in the ETT by the development of various levels of plastic strain corresponding to increasing values of DWTT energy. The impingement of the elastic to plastic strain overload capability dividing zone of DWTT energy (hatched band) with the OMTL indicates that at 60 to 80-ksi YS most materials should be expected to propagate fractures at elastic stress levels. Between 50 to 60-ksi YS range, optimized alloys if well cross-rolled may exceed this low level of fracture resistance. Below 50-ksi YS, a wide range of alloys that would require high plastic overloads for fracture propagation should be readily attainable. However, it must be pointed out that this high plastic overload capability is also accompanied by a relatively low intrinsic energy absorption in fracture propagation compared to steels and titanium. This is evident from the low DWTT energy values indexing plastic

strain requirements for fracture propagation in the aluminum FTID. Where large regions of a structure are subjected to plastic overloads, an engineering judgment must be made to determine if fracture safety is actually attained or if rupture is possible over a large area. For most structures where plastic overloads are confined to local geometric points that are stress indeterminate, the general engineering case analysis can be applied, that is, separation between the fracture-safe (plastic strain required for fracture propagation) and potentially fracture-propagating (fracture propagation at elastic stres levels) alloys.

DROP-WEIGHT TEAR TEST AND EXPLOSION TEAR TEST RESULTS

Six DWTT specimens of 7079-T6 alloy - three each in the RW and WR orientation - were tested in the 5000 ft-lb pendulum machine. The DWTT energy indicated in these tests were very low, as could be expected from the high YS (~68,000 psi)(2) of this alloy. Each of the WR specimens absorbed 111 ft-lb; two of the RW specimens absorbed 397 ft-lb, and the third absorbed 339 ft-lb. An interesting feature of these tests was the appearance of the fracture surfaces of the specimens. All of the specimens had the appearance of delamination (Fig. 29). The fracture surfaces of the RW specimens, which were more severely delaminated, were characterized by deep cracks and steps perpendicular to the fracture surface. The steps and possibly the cracks were probably formed by shear failure, or failure of large sheetlike precipitated films which are responsible for the high strength of the material.

Several ETT tests were conducted on 6061-T651 alloy (DWTT 750 ft-lb). In previous tests, this alloy has been tested extensively to establish the maximum amount of plastic strain which could be correlated with 750 ft-lb DWTT. A specimen which had been previously tested (Ref. 9, Fig. 14) was loaded a second time to approximately the same plastic strain level (7.3%). The flaw in the second test was the 10-in. flaw which developed in the first test of this specimen. The result of the second test was the complete fracturing of the specimen at one end (Fig. 30). Another 6061-T651 specimen was loaded to 8.2% plastic strain with the resulting fracture extending a total of 11-in. (Fig. 31); this result indicates that the 6061-T651 alloy has the capability to withstand plastic strain probably in excess of 9% without fracturing. A 2024-T4

specimen (DWTT 367 ft-lb) fractured completely when tested with load conditions that would have resulted in a 3.7% strain level (Fig. 32), indicating that the specific allowable strain level for this alloy is less than this value.

Specimens of 5086-H112 (DWTT 2026 ft-lb) were tested in the ETT with a very short fracture resulting from loading to 8.3% plastic strain (Fig. 33). The fracture extended into the plate material 3/4-in. at one end of the brittle weld flaw and barely extended into the plate material at the other end.

PLANE STRAIN FRACTURE TOUGHNESS TESTING OF TITANIUM

[C.N. Freed and R.J. Goode]

All practical engineering structures contain flaws or cracks which develop either during the forming or fabrication operations; such flaws are not always detected by inspection, or they may develop in service under conditions of low cycle fatigue. Therefore, to preclude catastrophic failure resulting from the presence of flaws, one of two conditions must be known at all times: 1. - the structural material is of sufficient fracture toughness so that the presence of these flaws will not trigger unstable crack propagation under the specific elastic or plastic loading conditions, i.e., material must undergo some degree of plastic straining with resultant minimal crack extension, or 2. - the exact level of stress (load plus residual) at critical sections of the structure and corresponding critical flaw sizes must not only be known, but it must also be assured that the flaws will be detected prior to and during service before they can ever reach critical size. Condition 2 becomes more important as requirements dictate the use of ultrahigh strength metals where small flaws can initiate failure at low levels of elastic strain.

The stress field at a crack tip may be defined by a single parameter, K, the stress intensity factor. The parameter is a function of the applied stress and the crack geometry. Determination of the plane-strain fracture toughness, K_{Ic}, as a material property will provide a measure of the resistance of a crack to unstable propagation under an applied stress as well as define the critical crack size for the material

MATERIALS AND PROCEDURE

The purpose of this investigation is to define the strength limitations of the practical application of fracture mechanics in determining valid fracture toughness numbers for the best (optimized) of the high and ultrahigh strength steels, titanium, and aluminum alloys. However, in this initial effort unalloyed titanium (T-17) was investigated, using single-edge-notched and side-notched specimens, since it was available in quantity and was known to be low in fracture toughness. This material had a yield strength (YS) of 83-ksi, ultimate tensile strength (UTS) of 101-ksi, 600 ft-lb drop-weight tear test (DWTT) energy, Charpy V (C_v) notch energy of 15 ft-lb at room temperature, and uniform through-thickness properties. The low DWTT energy value initially indicated that the plane strain fracture toughness (K_{Ic}) of this material should not be difficult to determine. It should be mentioned that these fracture toughness properties are considerably below what would be expected for an optimized alloy at this level of strength, but it does represent what would generally be expected of titanium alloys of above 140-ksi YS.

The effect of side-notching was also investigated. It was believed that the side-notch would constrain the plastic zone at the tip of the crack. This would allow 1. - smaller specimens to be used in order to obtain valid K_{Ic} values, and 2. - fracture mechanics numbers to be determined for materials of lower strength and higher toughness. Although an analytical analysis is not available for computing K_{Ic} from side-notched specimens, an empirical method has been evolved. As the results show, the use of the test data to provide valid K_{Ic} results at a temperature of interest hinges upon the development of an analytical method for the side-notched specimen.

TEST RESULTS

Before initiating the study, it was deemed necessary to ascertain the optimum specimen dimensions to provide valid results. In conjunction with Dr. J. Krafft (Mechanics Division, U.S. Naval Research Laboratory), tests were made to determine the relationship between the size of the plastic zone at the tip of the crack and the geometry of the edge-notched specimen. It soon became obvious that

for titanium with a low strength-to-toughness ratio the plastic zone would be so large as to necessitate specimens exceeding one inch in thickness at room temperature. As it was not desirable to test specimens over 1-in.-thick at the beginning of the study, the technique of side-notching was investigated.

The compressive stress-strain curve for 0.2% offset and the strain hardening exponent at temperatures between -320°F and 70°F was determined for T-17 with the use of compression plugs by Dr. Krafft. Using the techniques described in Ref. 16, the K_{I_C} values were calculated and a K_{I_C} versus test temperature curve was established. This curve is shown in Fig. 34. Two different size specimens were used in this study; these are shown in Fig. 35.

After machining and notching the specimens, a 0.01-in.-deep fatigue crack was introduced at the root of the notch. Plane strain conditions were established at temperatures of -24°F and below with these single-edge-notched specimens; "pop-in" or sharp changes in slope (crack initiation) was discernible on the load-deformation curve. The K_{I_C} values calculated for these temperatures were considered valid and, as seen in Fig. 34, define the same curve already established from the strain-hardening data. However, at the temperatures of 9°F and 60°F, crack instability could not be determined from the load-deformation curve and K_{I_C} values could not be calculated. The reason for this is explained by the lower curve in Fig. 34 which shows that the plastic zone radius (r_γ)* increases rapidly with temperature. In order to maintain the plane-strain condition in the specimen, r_γ must not exceed 0.25-in. for the 1-in.-thick specimen. An excessive plastic zone size will result in plastic flow at the root of the notch before fracture initiation and, consequently, no sharp demarcation or stress release is seen on the load-deformation curve.

A side-notched, 1-in.-thick specimen (Fig. 35) was tested at 60°F to determine if the constraint of the plastic zone by the side notch would be sufficient to maintain plane-strain conditions. The K_{I_C} value for this

---

* The plastic zone radius, $r_\gamma = (K_{I_C}/\delta_{ys})^2 \, 1/2\pi$. As both K_{I_C} and yield stress are temperature dependent, plastic zone size also varies with temperature.

specimen fell below that determined for the smooth specimens at -20°F and -40°F. This lower K_{Ic} value is understandable since the plastic zone even for the side-notched specimen was greater than one-fourth of the plate thickness. The value of the side notch may be seen in the load-deflection curves of Fig. 36. In curve "a", K_{Ic} calculated using maximum load would be excessively high, and a critical flaw size based on this number would be larger than the actual flaw size. In curve "b", the K_{Ic} is 9% low, and the size of a critical flaw based on this K_{Ic} might be considered on the conservative side. Thus, for cases in which the specimen thickness is less than $4r_y$, a lower K_{Ic} will be obtained from side-notched specimens. This means that side-notching can be utilized to constrain r_y for tougher materials than can be dealt with by conventional single-edge-notched specimens. A way of handling the added constraint of the plastic zone will have to be incorporated into whatever fracture mechanics analysis techniques are developed for calculating a valid K_{Ic} from this type specimen.

Small side-notched specimens were tested over a temperature range of -320°F to 75°F to determine the effect of the thickness of the unbroken ligament (Fig. 35) on the K_{Ic} values obtained Although the unbroken ligament was varied from 20 to 70% of the total specimen thickness, no significant difference was found in the K_{Ic} values at any temperature The technique for calculating K_{Ic} for side-notched specimens is described in Ref. 17.

The test results revealed that the plane strain fracture toughness values were valid over the temperature range of -320°F to -180°F. Above -180°F, the K_{Ic} values departed from the curve established with the 1-in.-thick specimens and the strain-hardening exponent, and became more or less constant, Fig. 34. Here again r_y exceeded one-quarter of the specimen thickness criteria (0.0625") although crack instability was detectable. Thus, it appears that side-notching does not change the specimen thickness requirement even though it does extend the range of temperature at which crack instability can be determined.

The effect of orientation on K_{Ic} is shown in Fig. 37 for T-17. The upper curve, which is the same one shown in Fig. 34, is the RW (transverse fracture direction and the lower, the WR (longitudinal fracture direction) with respect to rolling direction (5). Here it can readily be

seen that anisotropy is important and must be taken into account in measuring plane strain fracture toughness. The side-notched 1-in.-thick specimen provided an accurate measure of K_{I_C} up to +10°F. This is evident in that the values determined from -75°F to +10°F using the side-notched specimens increase in a linear manner with approximately the same slope as the specimens broken at lower temperatures which were not side-notched. Again, at 60°F the K_{I_C} determination for the WR specimen is lower even though crack instability was observed since r_y exceeded one-quarter of the specimen thickness.

DISCUSSION

At the beginning of this study, it was considered that the room temperature plane strain fracture toughness could be determined for titanium material with as low a DWTT energy as T-17 possessed. However, this has not been the case with T-17; the 600 ft-lb DWTT energy corresponds to the DWTT energy of an optimized (deduced from OMTL curve) titanium alloy of about 150-ksi YS at the same 1-in. thickness. Limited data developed to date at the 150-ksi YS level for optimized material indicates that the ductility of the high strength alloy may be as much as 50% lower than the ductility of unalloyed titanium at 83-ksi, 10% elongation versus 25% elongation, respectively. Whether this, or some other material property, has any bearing upon the difficulties encountered with T-17 is not known at this time. Work currently in progress on "optimized" or "nearly optimized" alloys ranging in strength from about 110-ksi YS to 180-ksi YS indicates that a measure of crack instability is detectable at room temperature over most of this range if side-notching is used. However, if the K_{I_C} calculated from side-notched specimens is found to be low (when the plastic zone radius is greater than one-quarter the thickness of the specimen), the usefulness of side-notching will be seriously impaired. Therefore, the development of an analytical means for treating side-notched specimens is imperative. It must be remembered that for optimized materials having a level of fracture toughness which requires side-notching techniques for K_{I_C} determinations, plastic straining will probably occur in the presence of reasonably sized flaws. For these materials, simpler and less expensive tests are available to measure fracture toughness, and K_{I_C} values per se would be of academic interest.

REFERENCES

1. Puzak, Lloyd, Lange, Goode, Huber, Dahlberg and Beachem, "Metallurgical Characteristics of High Strength Structural Materials (First Quarterly Report)," NRL Memorandum Report 1438, June 30, 1963

2. Goode, Huber, Howe, Judy, Crooker, Morey, Lange, Puzak, and Lloyd, "Metallurgical Characteristics of High Strength Structural Materials (Fourth Quarterly Report)," NRL Report 6137, June 1964

3. Pellini, W.S., and Puzak, P.P., "Factors that Determine the Applicability of High Strength Quenched and Tempered Steels to Submarine Hull Construction," NRL Report 5892, December 5, 1962

4. Huber, R.W., and Goode, R.J., "Fracture Toughness Tests for Titanium Alloy Plate and Forgings," NRL Report 6228, April 21, 1965

5. ASTM Materials and Research Standards, Vol. 1, No. 5, May 1961

6. Pellini, W.S., Goode, R.J., Puzak, P.P., Lange, E.A., and Huber, R.W., "Review of Concepts and Status of Procedures for Fracture-Safe Design of Complex Welded Structures Involving Metals of Low to Ultra-High Strength Levels," NRL Report 6300, June 1965

7. Crooker, Morey, Lange, Judy, Freed, Goode, Puzak, Lloyd, Huber, Howe, and Pellini, "Metallurgical Characteristics of High Strength Structural Materials (Fifth Quarterly Report)," NRL Report 6196, September 1964

8. "Grain Size Control in Ti-7Al-2Cb-1Ta Type Alloys," ITT Research Institute, Final Report, Contract N600(61533)59850

9. Pellini, Goode, Huber, Howe, Judy, Puzak, Lloyd, Lange, DeFelice, Crooker, Morey, Chapin, and McGeady, "Metallurgical Characteristics of High Strength Structural Materials (Sixth Quarterly Report)," NRL Report 6258, December 1964

10. Dorshu, K.E., and Lesnewich, A., "Development of a Filler Metal for a High Toughness Alloy Plate Steel with a Minimum Yield Strength of 140 KSI," Air Reduction Sales Co., Murray Hill, N.J.

11. Puzak, Lloyd, Goode, Huber, Howe, Crooker, Lange, and Pellini, "Metallurgical Characteristics of High Strength Structural Materials (Third Quarterly Report)," NRL Report 6086, January 1964

12. Crooker, Morey, and Lange, "Low Cycle Fatigue Crack Propagation Characteristics of Monel 400 and Monel K-500 Alloys," NRL Report 6218 (publication pending)

13. Crooker, Morey, and Lange, "Report of NRL Progress," June 1964, pp. 30-33

14. Carman, C.M., Katlin, J.M., and Paris, P.C., "Low Cycle Fatigue Properties of High Strength Solid Propellant Rocket Motor Materials," Fourth Maraging Steel Project Review, Air Force Materials Laboratory, Dayton, Ohio, June 1964

15. Hanna, G.L., Troiano, A.R., and Steigerwald, E.A., "A Mechanism for the Embrittlement of High-Strength Steels by Aqueous Environments," ASM TRANS QUARTERLY, September 1964

16. Krafft, J.M., "Correlation of Plane Strain Crack Toughness with Strain Hardening Characteristics of a Low, a Medium, and a High Strength Steel," Applied Materials Research, pp. 88-101, April 1964

17. Freed, C.N., and Krafft, J.M., "Effect of Side Notching on Measurements of Plane Strain Fracture Toughness," Presented to the Committee on Fracture Testing of High Strength Metallic Materials, Washington, D.C., May 12, 1965.

Table 1
Test Data for Solution Annealing and Aging Treatments
on the Alloy Ti-6Al-4Zr-2Mo (T-55)

(β transus = 1840°F ± 15°F)

Solution Heat Treatment	Aging Heat Treatment	Longitudinal (RW) C_v-notch Impact Energy (ft-lb)		Transverse (WR) C_v-notch Impact Energy (ft-lb)		.2% Offset YS (ksi)	UTS (ksi)	Elong. (%)	RA (%)
		-80°F	+32°F	-80°F	+32°F				
As received condition		18.5	25.5	18.5	26.5	121.4(L) 111.8(T)	125.0(L) 131.0(T)	10.7 9.3	29.5 29.4
1800°F-1 Hr.-W.Q.		15.0	23.0	17.0	16.0				
1800°F-1 Hr.-W.Q.	1100°F-2 Hr.-A.C.	13.5	11.5	13.0	12.0	152.2(L) 160.1(T)	168.0(L) 174.2(T)	4.3 4.3	8.2 7.5
1800°F-1 Hr.-W.Q.	1200°F-2 Hr.-A.C.	12.0	15.5	13.0	16.5	150.9(L) 150.5(T)	162.9(L) 163.0(T)	5.0 5.0	12.4 10.6
1750°F-1 Hr.-W.Q.		21.5	22.0	17.5	21.5	116.6(L) 118.6(T)	148.2(L) 148.2(T)	10.0 9.3	14.9 21.2
1750°F-1 Hr.-W.Q.	1100°F-2 Hr.-A.C.	14.0	17.5	15.5	20.0	138.7(L) 153.8(T)	156.8(L) 169.0(T)	4.3 5.7	8.2 14.2
1750°F-1 Hr.-W.Q.	1200°F-2 Hr.-A.C.	21.0	27.5	20.0	26.5	134.2(L) 141.0(T)	148.2(L) 153.8(T)	4.3 7.1	9.9 19.4
1700°F-1 Hr.-W.Q.		21.0	26.5	21.0	26.5	99.1(L) 118.6(T)	136.4(L) 145.9(T)	12.1 12.1	25.2 23.5
1700°F-1 Hr.-W.Q.	1100°F-2 Hr.-A.C.	15.5	20.0	15.0	19.5	134.4(L) 132.4(T)	149.5(L) 148.2(T)	5.7 5.0	14.2 13.6
1700°F-1 Hr.-W.Q.	1200°F-2 Hr.-A.C.	22.5	27.0	20.0	26.5	130.9(L) 135.5(T)	144.3(L) 146.9(T)	7.9 10.7	16.5 26.2
1650°F-1 Hr.-W.Q.		19.5	29.5	22.0	30.5	106.4(L) 106.1(T)	137.3(L) 141.6(T)	10.7 10.7	28.5 29.5
1650°F-1 Hr.-W.Q.	1100°F-2 Hr.-A.C.	16.5	23.0	17.5	23.0	127.0(L) 131.9(T)	140.1(L) 141.4(T)	6.4 9.3	14.1 17.1
1650°F-1 Hr.-W.Q.	1200°F-2 Hr.-A.C.	20.5	30.0	24.0	28.0	126.8(L) 127.5(T)	138.3(L) 134.7(T)	9.3 8.6	24.0 18.8
1800°F-1 Hr.-A.C.		25.0	41.0	28.0	39.5				
1800°F-1 Hr.-A.C.	1100°F-2 Hr.-W.Q.	25.0	36.0	23.0	30.5	120.6(L) 124.8(T)	131.8(L) 136.4(T)	7.9 10.0	24.5 19.5
1800°F-1 Hr.-A.C.	1200°F-2 Hr.-W.Q.	27.0	40.0	33.5	38.5	119.6(L) 125.8(T)	131.4(L) 133.7(T)	9.3 10.0	24.5 21.7
1750°F-1 Hr.-A.C.		27.0	34.5	28.0	37.5	116.0(L) 116.4(T)	133.0(L) 132.0(T)	12.1 11.4	30.8 24.7
1750°F-1 Hr.-A.C.	1100°F-2 Hr.-W.Q.	23.0	32.5	26.5	37.5	118.2(L) 122.9(T)	132.4(L) 134.4(T)	10.0 10.7	24.0 26.7
1750°F-1 Hr.-A.C.	1200°F-2 Hr.-W.Q.	24.5	32.0	24.5	37.5	118.2(L) 121.9(T)	128.5(L) 131.8(T)	9.3 10.7	31.1 26.2
1700°F-1 Hr.-A.C.		25.0	34.0	31.5	36.0	110.4(L) 114.5(T)	131.3(L) 130.5(T)	12.1 11.4	30.8 34.6
1700°F-1 Hr.-A.C.	1100°F-2 Hr.-W.Q.	27.0	34.0	26.0	30.5	115.1(L) 119.6(T)	128.6(L) 129.8(T)	11.4 10.7	28.5 36.4
1700°F-1 Hr.-A.C.	1200°F-2 Hr.-W.Q.	25.5	36.0	23.0	32.0	119.9(L) 121.9(T)	130.4(L) 131.1(T)	10.7 10.7	31.6 31.1

(L) = Longitudinal direction (RW)
(T) = Transverse direction (WR)

Table 2
Test Data for Solution Annealing and Aging Treatments on the Alloy Ti-6Al-4Zn-2Sn-.5Mo-.5V (T-68) (β transus = 1865°F ± 15°F)

Solution Heat Treating	Aging Heat Treatment	Longitudinal (RW) C_v-notch Impact Energy (ft-lb)		Transverse (WR) C_v-notch Impact Energy (ft-lb)		.2% Offset YS (ksi)	UTS (ksi)	Elong. (%)	RA (%)
		-80°F	+32°F	-80°F	+32°F				
As received condition		20.0		18.0		113.5(L) 124.0(T)	121.1(L) 130.2(T)	10.7 10.7	30.0 28.4
1850°F-1 Hr.-W.Q.		18.5	24.5	20.0	26.0	122.7(L) 124.8(T)	150.9(L) 154.2(T)	6.4 6.4	8.8 11.2
1850°F-1 Hr.-W.Q.	1100°F-2 Hr.-A.C.	20.0	19.0	14.5	19.0	140.9(L) 139.5(T)	155.8(L) 153.5(T)	5.7 4.3	13.7 6.9
1850°F-1 Hr.-W.Q.	1200°F-2 Hr.-A.C.	16.0	22.5	16.5	19.0	137.9(L) 137.9(T)	150.2(L) 150.5(T)	5.7 5.7	8.2 9.3
1800°F-1 Hr.-W.Q.		21.5	29.5	27.0	49.0				
1800°F-1 Hr.-W.Q.	1100°F-2 Hr.-A.C.	21.0	29.0	24.5	35.5	141.0(L) 144.9(T)	152.5(L) 156.5(T)	7.9 7.1	14.9 12.3
1800°F-1 Hr.-W.Q.	1200°F-2 Hr.-A.C.	20.5	28.5	23.0	30.5	131.1(L) 137.8(T)	141.0(L) 147.6(T)	7.1 6.4	23.5 18.8
1750°F-1 Hr.-W.Q.		23.0	30.0	27.0	35.0	119.9(L) 124.7(T)	141.6(L) 144.3(T)	7.9 7.9	25.2 25.0
1750°F-1 Hr.-W.Q.	1100°F-2 Hr.-A.C.	20.5	28.5	24.5	30.0	128.6(L) 134.1(T)	137.9(L) 137.7(T)	5.7 7.9	15.4 15.9
1750°F-1 Hr.-W.Q	1200°F-2 Hr.-A.C.	22.0	26.5	26.0	34.0	127.0(L) 132.2(T)	136.6(L) 142.0(T)	6.4 7.9	23.5 22.8
1700°F-1 Hr.-W.Q.		22.5	27.5	23.0	37.5	109.9(L) 120.2(T)	124.7(L) 133.4(T)	9.3 10.7	32.6 32.7
1700°F-1 Hr.-W.Q.	1100°F-2 Hr.-A.C.	22.5	32.0	22.5	29.5	126.0(L) 132.1(T)	135.3(L) 140.3(T)	10.0 9.3	23.5 22.3
1700°F-1 Hr.-W.Q.	1200°F-2 Hr.-A.C.	21.0	28.5	26.5	32.5	120.4(L) 120.9(T)	126.3(L) 127.1(T)	9.3 9.3	28.0 29.0
1850°F-1 Hr.-A.C.		23.0	36.0	27.5	30.5	118.4(L) 120.0(T)	130.6(L) 132.0(T)	10.0 10.0	22.9 20.2
1850°F-1 Hr.-A.C.	1100°F-2 Hr.-W.Q.	26.5	30.5	25.5	29.0	121.2(L) 121.7(T)	131.2(L) 131.3(T)	10.0 10.0	26.4 25.2
1850 F-1 Hr.-A.C.	1200°F-2 Hr.-W.Q.	23.0	33.0	24.5	34.0	121.7(L) 122.7(T)	131.6(L) 132.3(T)	9.3 10.7	24.1 24.1
1800°F-1 Hr.-A.C.		31.0	34.5	27.0	45.5				
1800°F-1 Hr.-A.C.	1100°F-2 Hr.-W.Q.	30.0	37.5	26.5	38.0	119.4(L) 120.0(T)	126.0(L) 131.0(T)	9.3 9.3	26.8 30.6
1800°F-1 Hr.-A.C.	1200°F-2 Hr.-W.Q.	23.0	33.0	27.0	45.5	113.7(L) 119.4(T)	121.7(L) 127.6(T)	10.7 10.0	23.5 30.0
1750°F-1 Hr.-A.C.		25.5	37.5	28.0	35.0	108.0(L) 118.4(T)	124.5(L) 131.0(T)	10.7 10.7	29.5 30.0
1750°F-1 Hr.-A.C.	1100°F-2 Hr.-W.Q.	25.0	38.5	27.0	44.5	108.1(L) 118.0(T)	117.0(L) 127.3(T)	10.7 11.4	43.9 34.9
1750°F-1 Hr.-A.C.	1200°F-2 Hr.-W.Q.		37.5	27.0	36.5	118.0(L) 119.0(T)	126.7(L) 128.0(T)	10.[illegible] 10.7	28.5 30.1
1700°F-1 Hr.-A.C.		28.0	36.0	25.0	30.0	109.4(L) 107.0(T)	123.8(L) 119.9(T)	12.1 10.7	34.8 41.4
1700°F-1 Hr.-A.C.	1100°F-2 Hr.-W.Q.	24.5	32.5	27.0	37.5	116.9(L) 124.0(T)	127.1(L) 132.3(T)	10.0 12.1	21.2 25.2
1700°F-1 Hr.-A.C.	1200°F-2 Hr.-W.Q.	23.5	30.0	23.5	37.5	117.5(L) 117.6(T)	125.2(L) 124.6(T)	10.0 10.0	28.0 32.3

(L) = Longitudinal direction (RW)
(T) = Tranverse direction (WR)

Table 3
Average Strength of Heat Treated Drop-Weight Tear
Specimens of the Alloy Ti-6Al-2Mo (T-22)

0.313-in. Diam. Tensil Specimen No.	YS (ksi)	UTS (ksi)	Elong. (%)	RA (%)	DWTT @ +30°F (ft-lb)	Heat Treatment
T-22 #DT1	118.8	124.7	14.3	38.4	3729(L)	1750°F-1 Hr.-A.C. -
T-22 #DT2	118.8	123.4	12.9	37.8		1100°F-2 Hr.-W.Q.
Average	118.8(T)	124.0(T)	13.6	38.1		
T-22 (Pre-machined)	125.9(L)	131.7(L)	12.5	35.7		1750°F-1 Hr.-A.C. -
	123.0(T)	131.2(T)	12.9	32.7		1100°F-2 Hr.-W.Q.
T-22 #EL1	120.0	124.5	13.6	43.2	3333(L)	1750°F-1 Hr.-A.C. -
T-22 #EL2	118.0	121.9	13.6	41.2		1100°F-4 Hr.-W.Q.
Average	119.0(L)	123.2(L)	13.6	42.2		
T-22 (Pre-machined)	127.3(L)	131.6(L)	12.9	41.5		1750°F-1 Hr.-A.C. -
						1100°F-4 Hr.-W.Q.
T-22 #ET1	117.5	124.0	15.0	42.8		1750°F-1 Hr.-A.C. -
T-22 #ET2	114.8	122.9	14.3	42.7		1100°F-4 Hr.-W.Q.
Average	116.1(T)	123.4(T)	14.6	42.8		
T-22 (Pre-machined)	122.4(T)	129.0(T)	13.2	35.0		1750°F-1 Hr.-A.C. -
						1100°F-4 Hr.-W.Q.

(L) Longitudinal direction (RW) (7)
(T) Transverse direction (WR) (7)

Table 4
Mechanical Properties of 5Ni-Cr-Mo-V Plates and Weld Metals
Used for Explosion Bulge Specimens
(Determined by United States Steel Corporation Research Laboratory)

Specimen	0.2% YS (ksi)	UTS (ksi)	El. in 2 in. (%)	R.A. (%)	C_v @ 30°F (ft-lb)
1-in.-plate (5Ni-Cr-Mo-V)	136		21.0		99
Airco weld metal (covered stick electrode)	144	147	18.2	58	46
Arcos weld metal (covered stick electrode)	141	152	16.8	55	33
McKay weld metal (covered stick electrode)	145	155	14.0	37	39
1-in.-plate (5Ni-Cr-Mo-V)	133		20.5		95
Airco weld metal (MIG interrupted-arc)	140	156	17.8	62	55
Linde weld metal (MIG interrupted-arc)	135	147	18.2	59	62

NOTE: All 0.505-in. diameter tensile specimens except Airco MIG interrupted-arc - 0.357-in. diameter.

Table 5
Explosion Bulge Testing of 140 Yield Strength Weld
Metal Tested with Bulge Area Weld Crown Intact

Specimen	Total Shots (7-lb Pentolite 15-in. Stand-off)	First Visible Fracture	Thickness Reduction Preceding Shot	Bulge Depth Preceding Shot (inch)
McKay (stick electrode)	6	6th shot - 1-inch toe crack at edge of weld	14.4%	3.3
Arcos (stick electrode)	6	6th shot - 1/2-inch toe crack at edge of weld	13.1%	3.2
Airco (stick electrode)	5	4th shot - 4-inch crack at toe of weld. 3-inch crack in weld	9.2%	2.5
Airco #1 (MIG interrupted-arc, vertical-up)	6	6th shot - 4 transverse weld cracks - 6-inch toe cracks each edge of weld	12.2%	3.3
Airco #2 (MIG interrupted-arc, vertical-up)	4	2nd shot - 6-inch and 4-inch toe cracks along each side	4.4%	1.54
Linde (MIG interrupted-arc, vertical-up)	4	2nd shot - transverse cracks in weld	4.5%	1.50

Table 6
Test Data for Explosion Bulge Test Specimens of Experimental
180-ksi Yield Strength Maraging Steel Weldments

Bulge Specimen	Plate No.	Weld Metal No.	Treatment
Number 1	H-7	WMA-1	Aged 18 hours at 825°F after welding
Number 2	H-8	WMA-2	Aged 6 hours at 950°F after welding

Bulge Specimen Properties after Aging

Plate and Weld Number	Hardness (R_c)	0.505-in. Diam. Tension Data				C_v @ 30°F (ft-lb)	C_v @ Room Temp. (ft-lb)	Direction of Test	Lab. Data	Remarks
		.2% YS (ksi)	UTS (ksi)	El. in 2 in. (%)	R.A. (%)					
Plate #H-7	43/44	192.1	199.9	13.5	47.0	34	35	Weak*	NRL	Specimens removed from hold-down region of bulge sample.
Weld #WMA-1	34/36	–	–	–	–	–	–	–	NRL	
Weld #WMA-1	–	167.5	–	–	–	–	59	–	INCO	Transverse tension test - failure in weld metal.
Plate #H-8	41/42	178.9	183.4	17.0	64.6	57	58	Weak*	NRL	Specimens removed from hold-down region of bulge sample.
Plate #H-8	–	–	–	–	–	58	57	Strong†	NRL	
Weld #WMA-2	42/43	176.4	176.4	14.0	65.0	–	47	–	INCO	Transverse tension test - failure in heat-affected-zone (HAZ)
Weld #WMA-2	–	–	–	–	–	41	–	–	NRL	Specimens removed from hold-down region of bulge sample.
Plate #H-7	–	–	–	–	–	40	41	Weak*	NRL	Plate specimen blanks aged 3 hr. @ 900°F.
Plate #H-7	41/41.5	183.2	186.6	15.0	62.5	50	49	Strong†	NRL	
Plate #H-8	–	–	–	–	–	54	55	Weak*	NRL	Plate specimen blanks aged 3 hr. @ 900°F.
Plate #H-8	41/41.5	183.2	191.7	13.0	52.5	58	65	Strong†	NRL	

* Weak represents direction of primary rolling
† Strong represents 90° to direction of primary rolling

Table 7
Chemical Composition of High Strength Steels

Code	Material	% Composition by Weight								
		C	Mn	P	S	Si	Ni	Cr	Mo	V
G85	D6AC	.47	.80	.005	.006	.20	.54	1.18	1.04	.09
G98	4335	.38	.85	.008	.006	.39	1.65	.95	.36	.15

Table 8
Chemical Composition of High Strength Steels

Code	Material	0.505-in. Diameter Tensile Data			
		0.2% YS (ksi)	UTS (ksi)	El. in 2 in. (%)	R.A. (%)
G85	D6AC	212	229	12.0	44.6
G98	4335	215	244	10.5	41.3

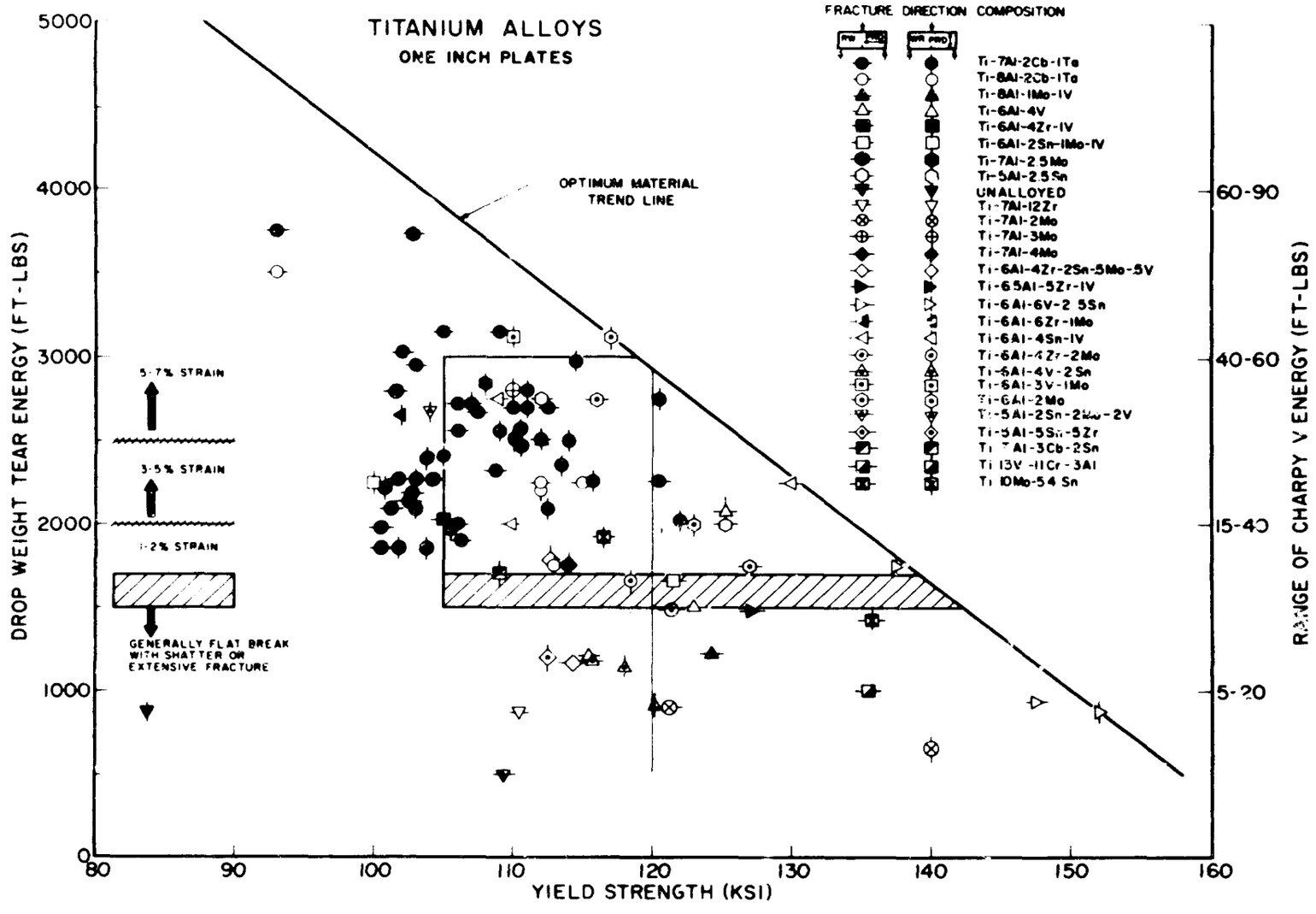

Fig. 1 - Fracture toughness index diagram for titanium. Correlates drop-weight tear test, Charpy V, explosion tear test, and yield strength data for 1-in.-thick titanium alloy plates. Optimum materials trend line indicates estimated highest level of strength for any given level of toughness.

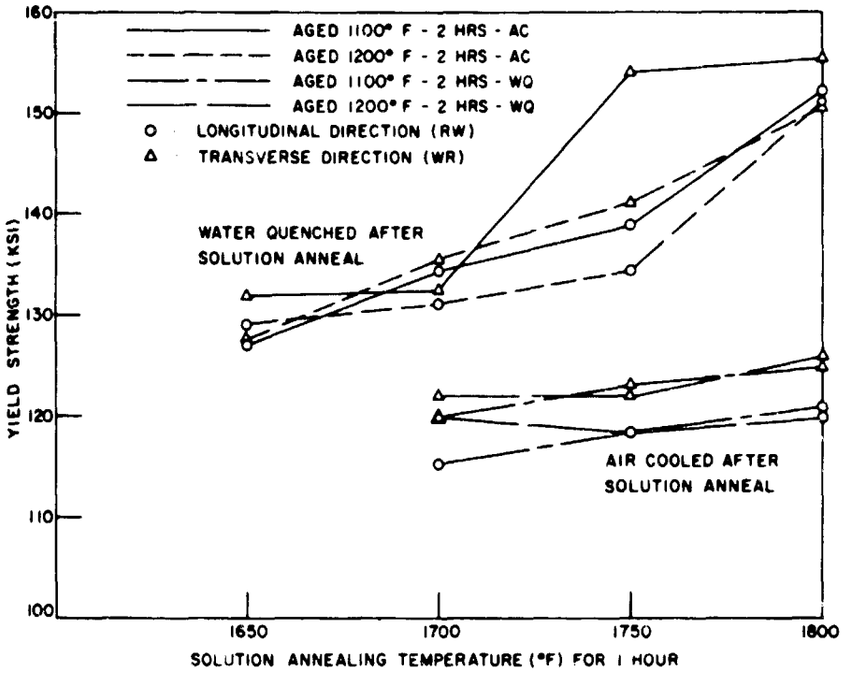

Fig. 2 - Effects of variations in solution annealing temperatures on the yield strength of the alloy Ti-6Al-4Zr-2Mo (T-55) with aging treatment

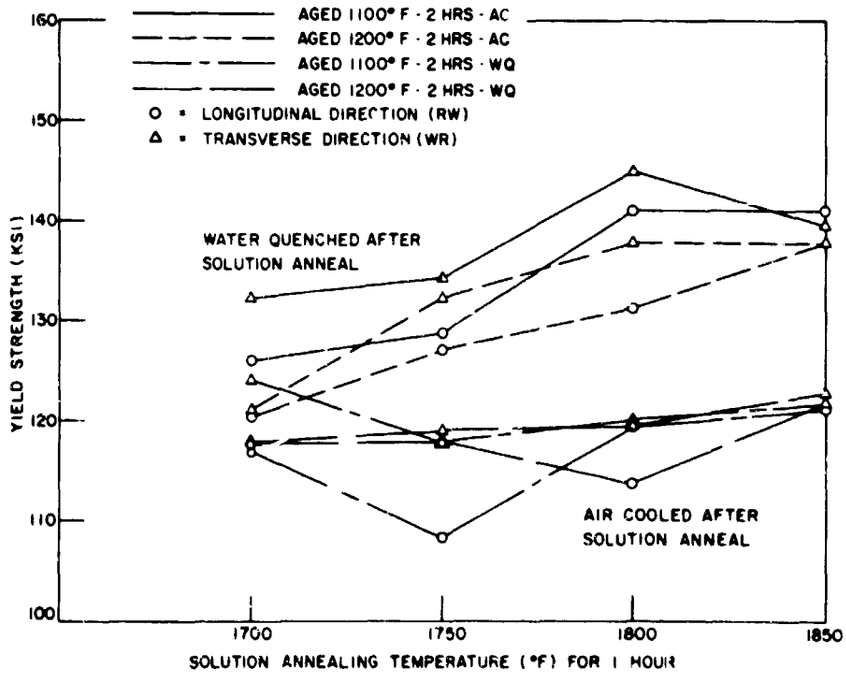

Fig. 3 - Effects of variations in solution annealing temperatures on the yield strength of the alloy Ti-6Al-4Zr-2Sn-.5Mo-.5V (T-68) with aging treatment

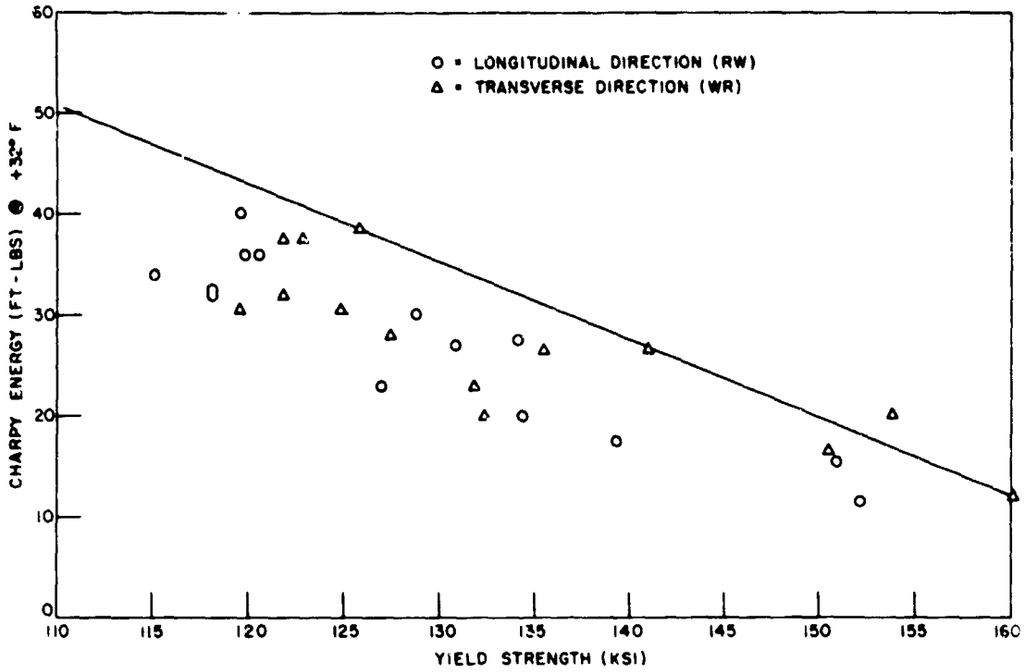

Fig. 4 - Summary of Charpy V energy and yield strength relationships for the alloy Ti-6Al-4Zr-2Mo (T-55)

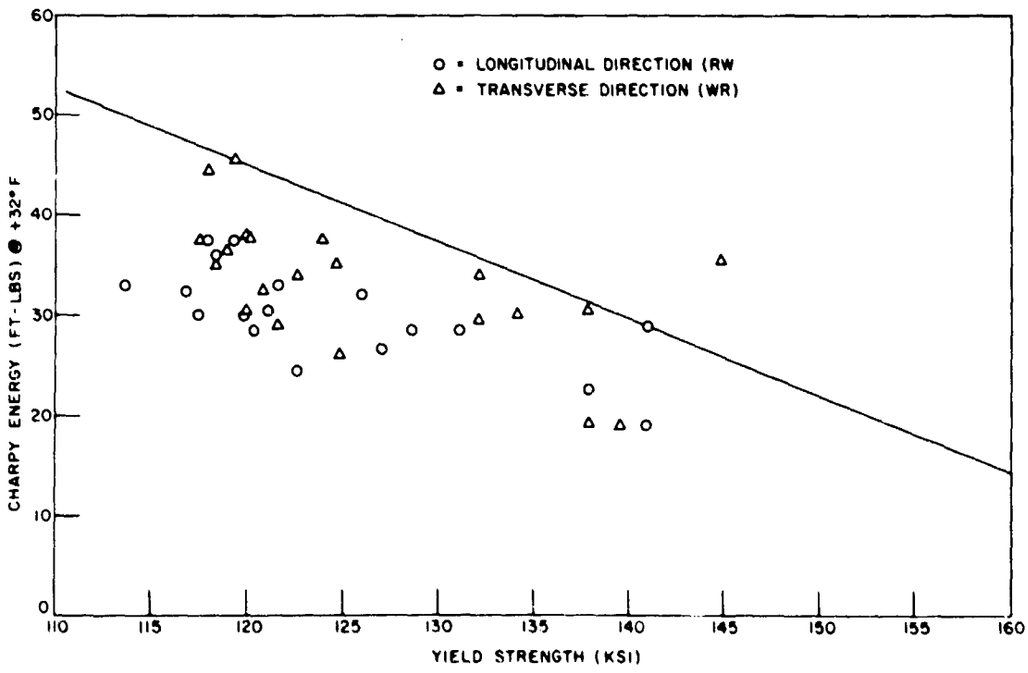

Fig. 5 - Summary of Charpy V energy and yield strength relationships for the alloy Ti-6Al-4Zr-2Sn-.5Mo-.5V (T-68)

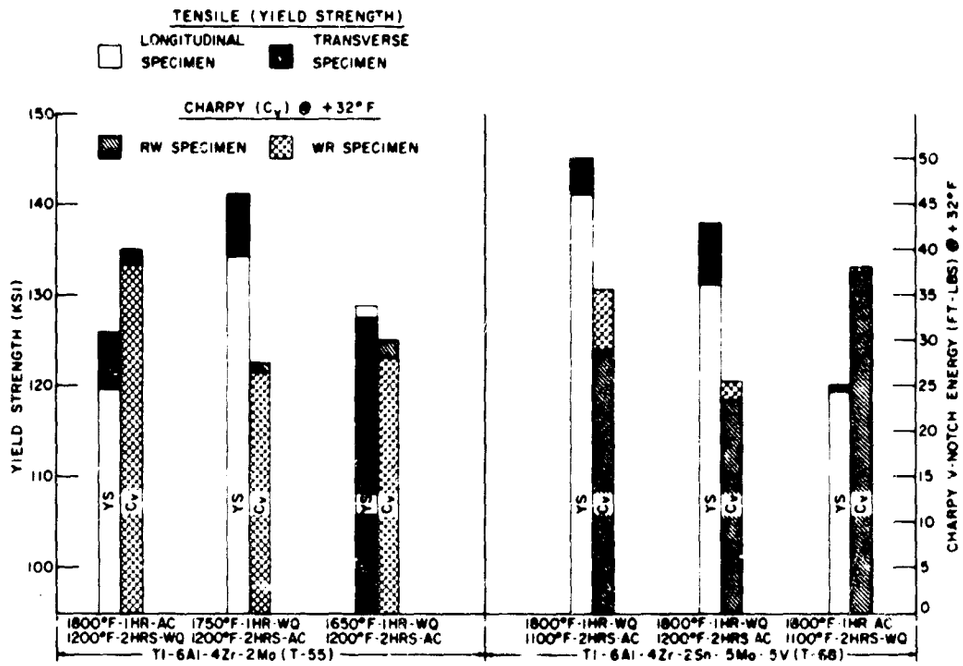

Fig. 6 - Effect of heat treatments on the Charpy V-notch energy of the alloys Ti-6Al-4Zr-2Mo (T-55) and Ti-6Al-4Zr-2Sn-.5Mo-.5V (T-68) in the 120-145-ksi yield strength range

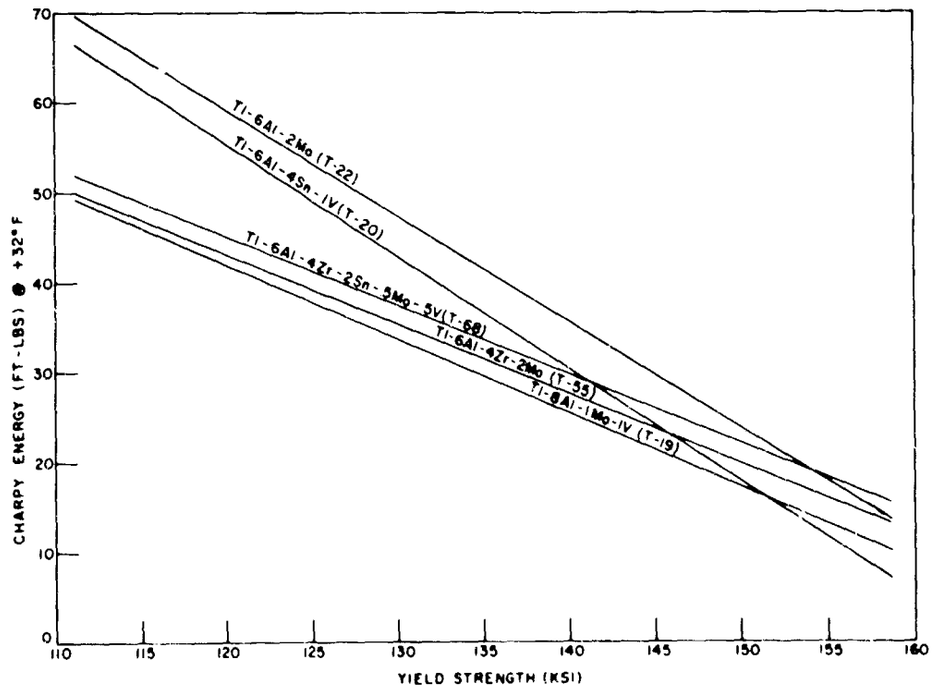

Fig. 7 - Summary of Charpy V energy and yield strength relationships for several titanium alloys

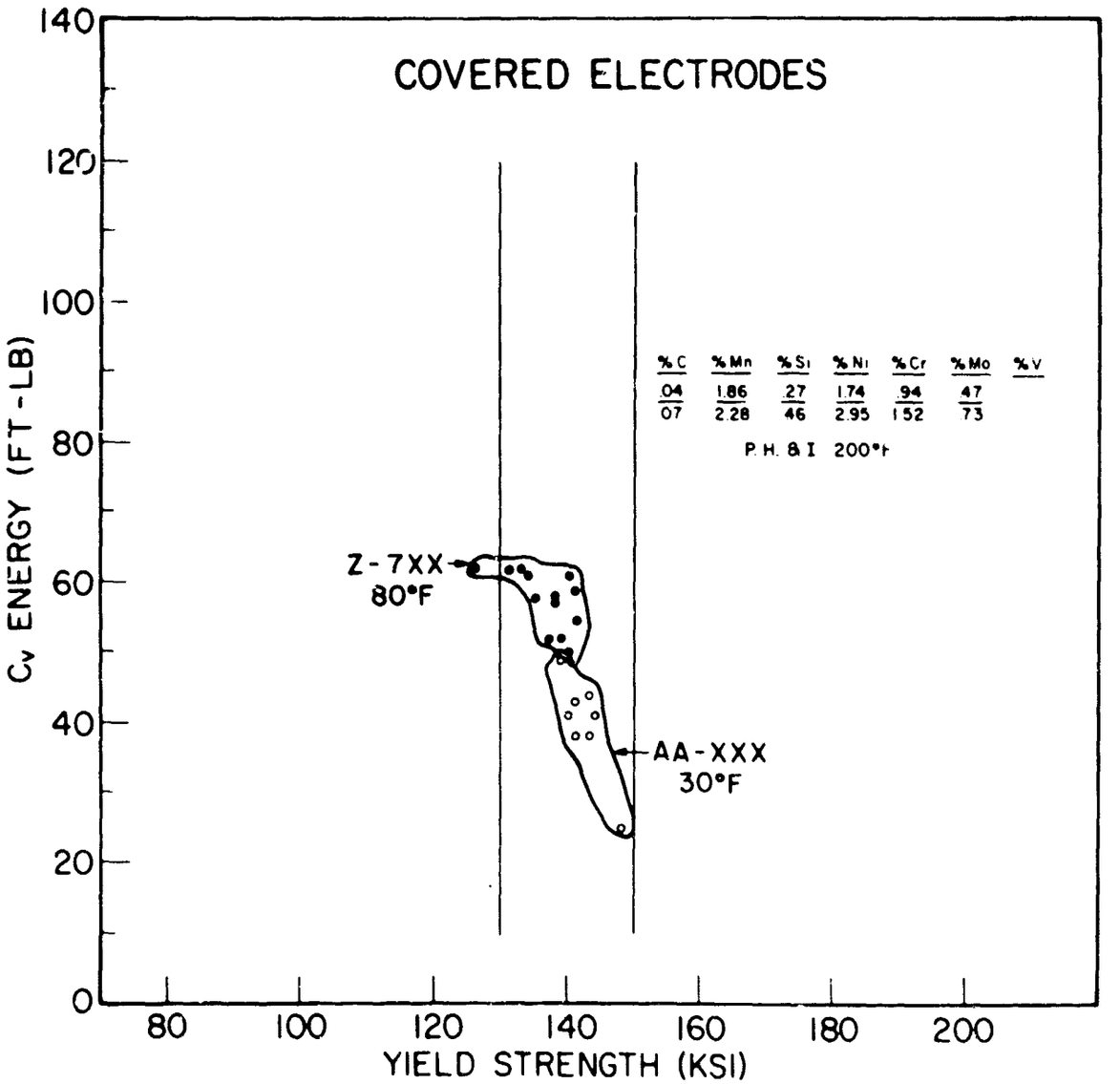

Fig. 8 - Charpy V and yield strength values developed with experimental covered stick welding electrodes

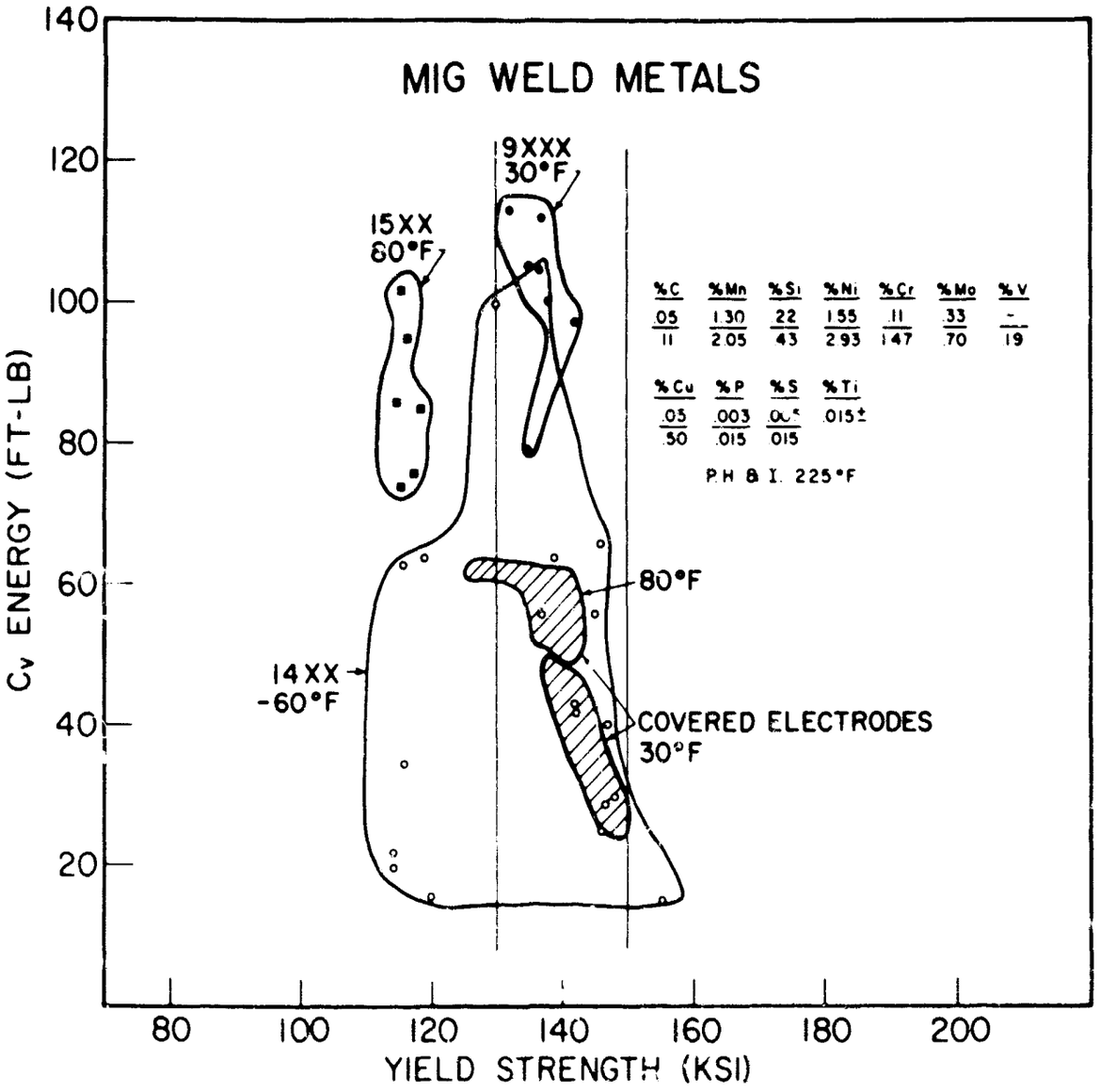

Fig. 9 - Charpy V and yield strength values developed with experimental MIG welding; data zones for stick electrodes from Fig. 1 added for comparison

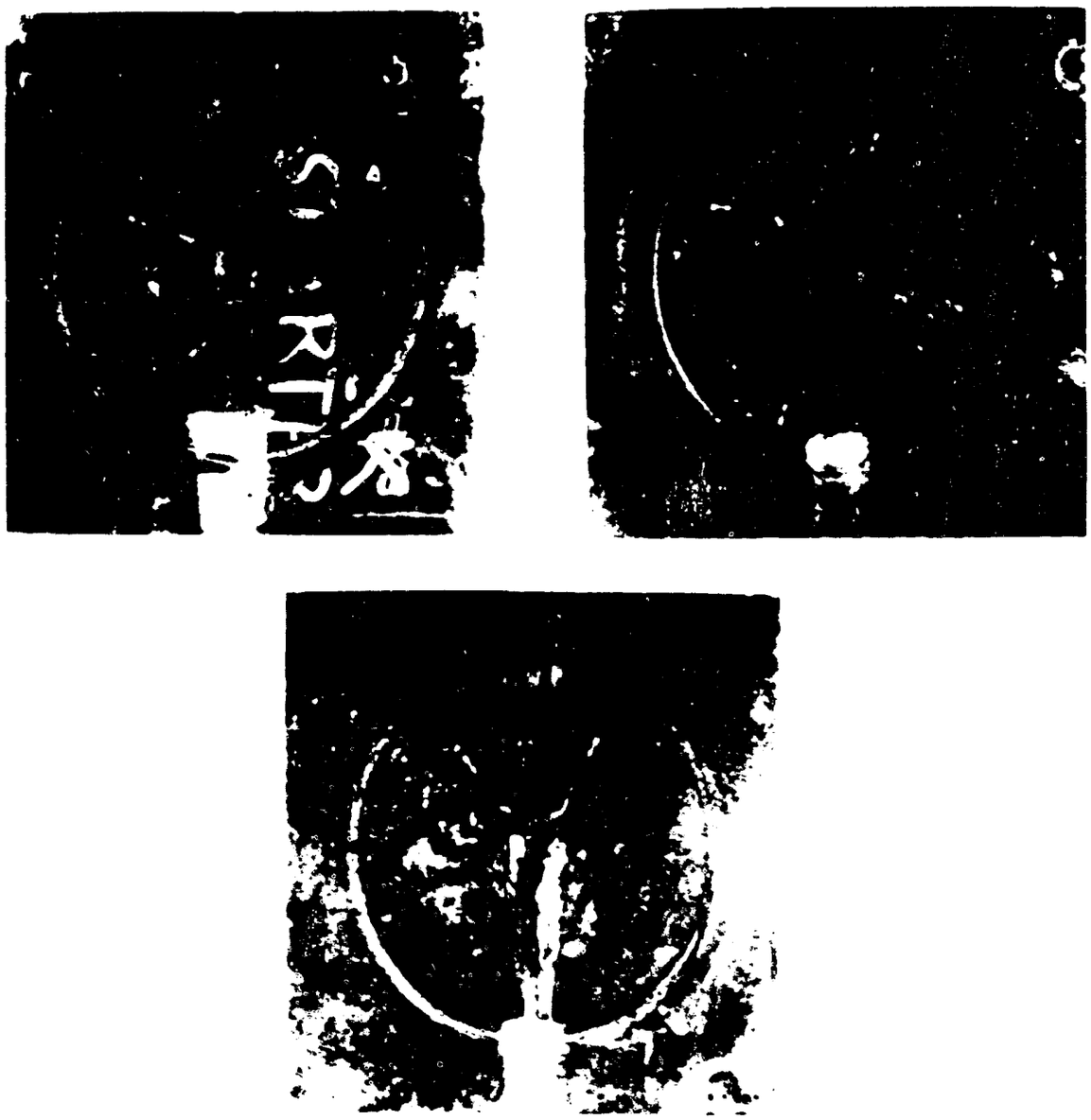

Fig. 10 - Crack-starter explosion bulge tests of 140-ksi yield strength covered stick electrode welds after two 7-lb Pentolite shots: upper left, Airco plate; upper right, McKay plates; lower, Arcos plate

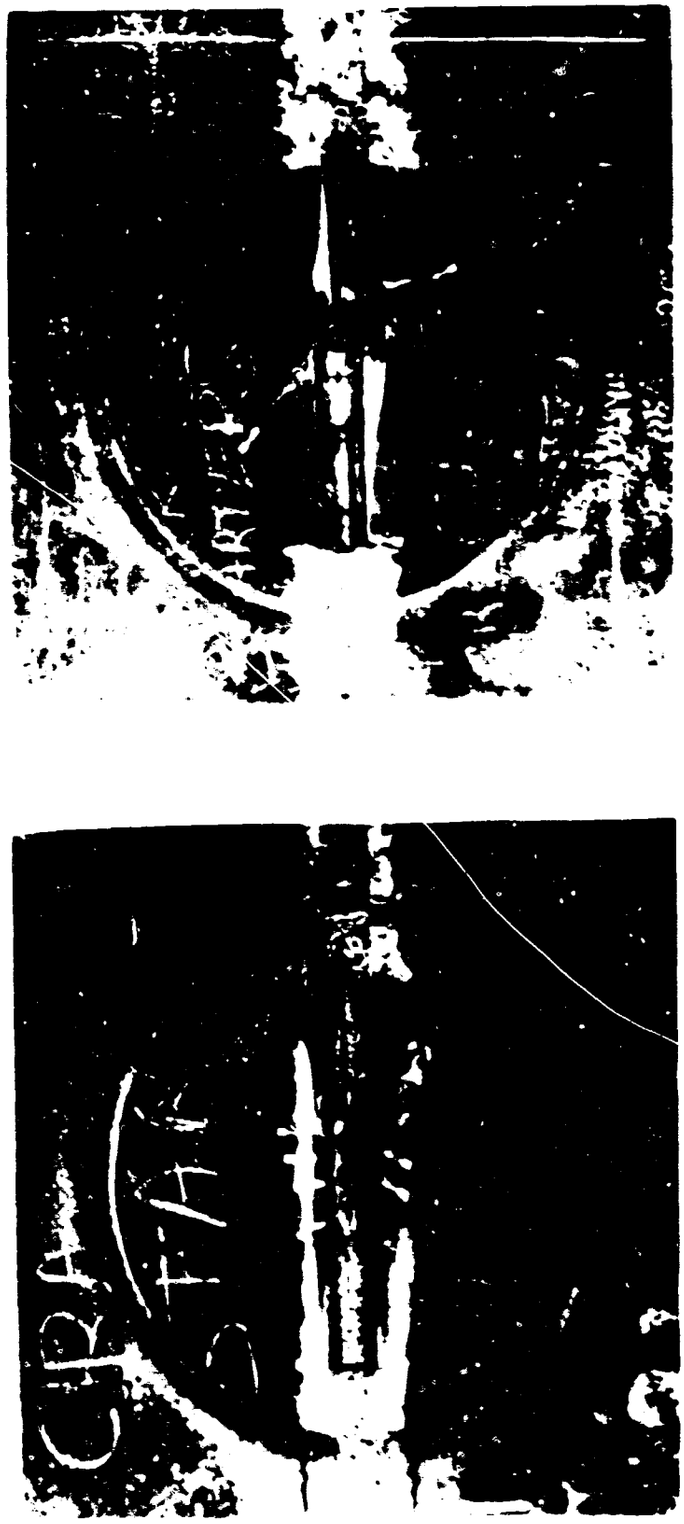

Fig. 11 - Crack-starter explosion bulge tests of MIG interrupted-arc vertical welds after two 7-lb Pentolite shots: upper, Airco plate; lower, Linde plate

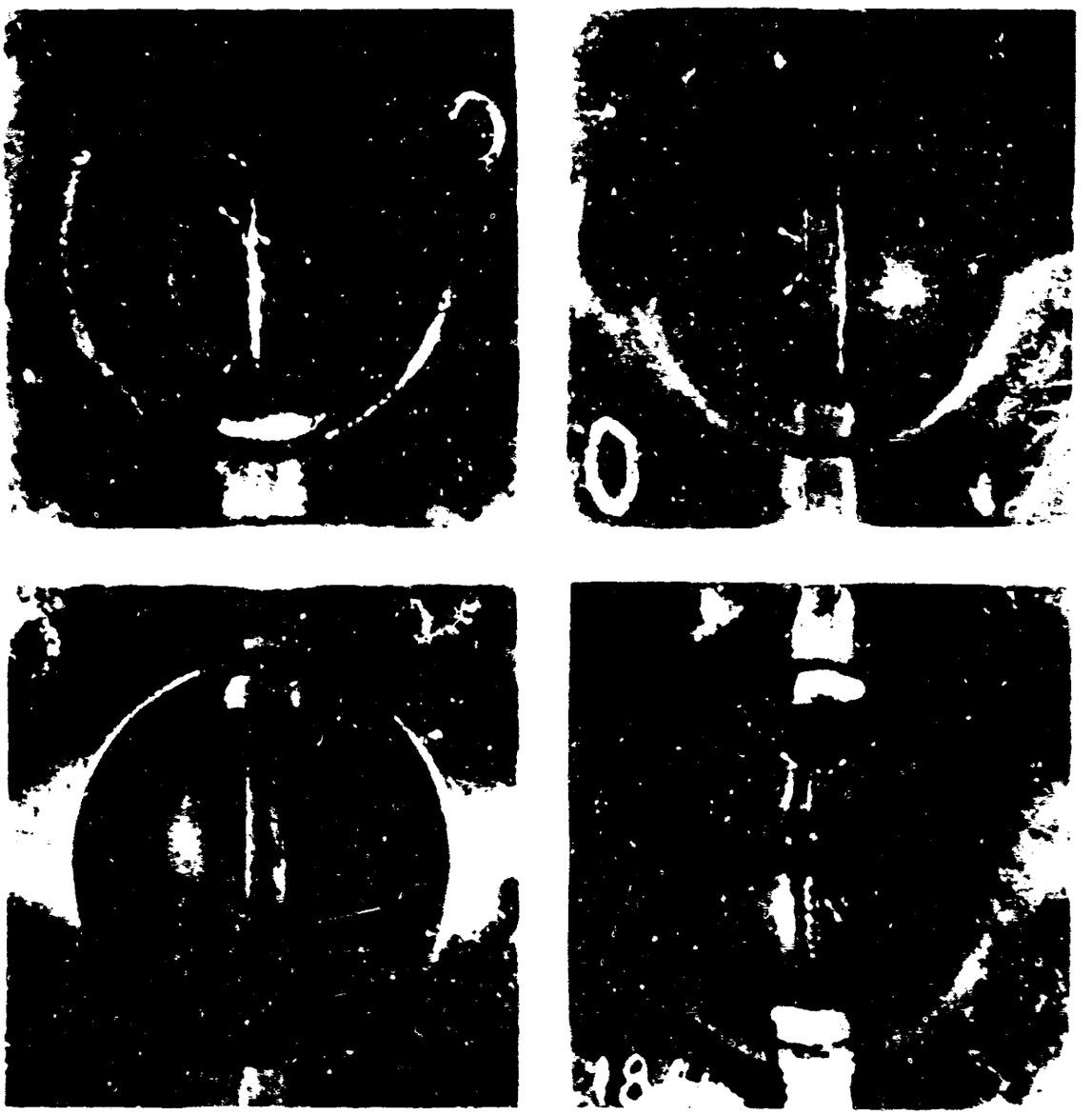

Fig. 12 - As-welded explosion bulge tests of 140-ksi yield strength welds: upper left, Airco covered stick electrode after 5 shots; upper right, McKay covered stick electrode after 6 shots; lower left, Arcos covered stick electrode after 6 shots; and lower right, Airco MIG interrupted-arc (vertical-up) weld after 6 shots

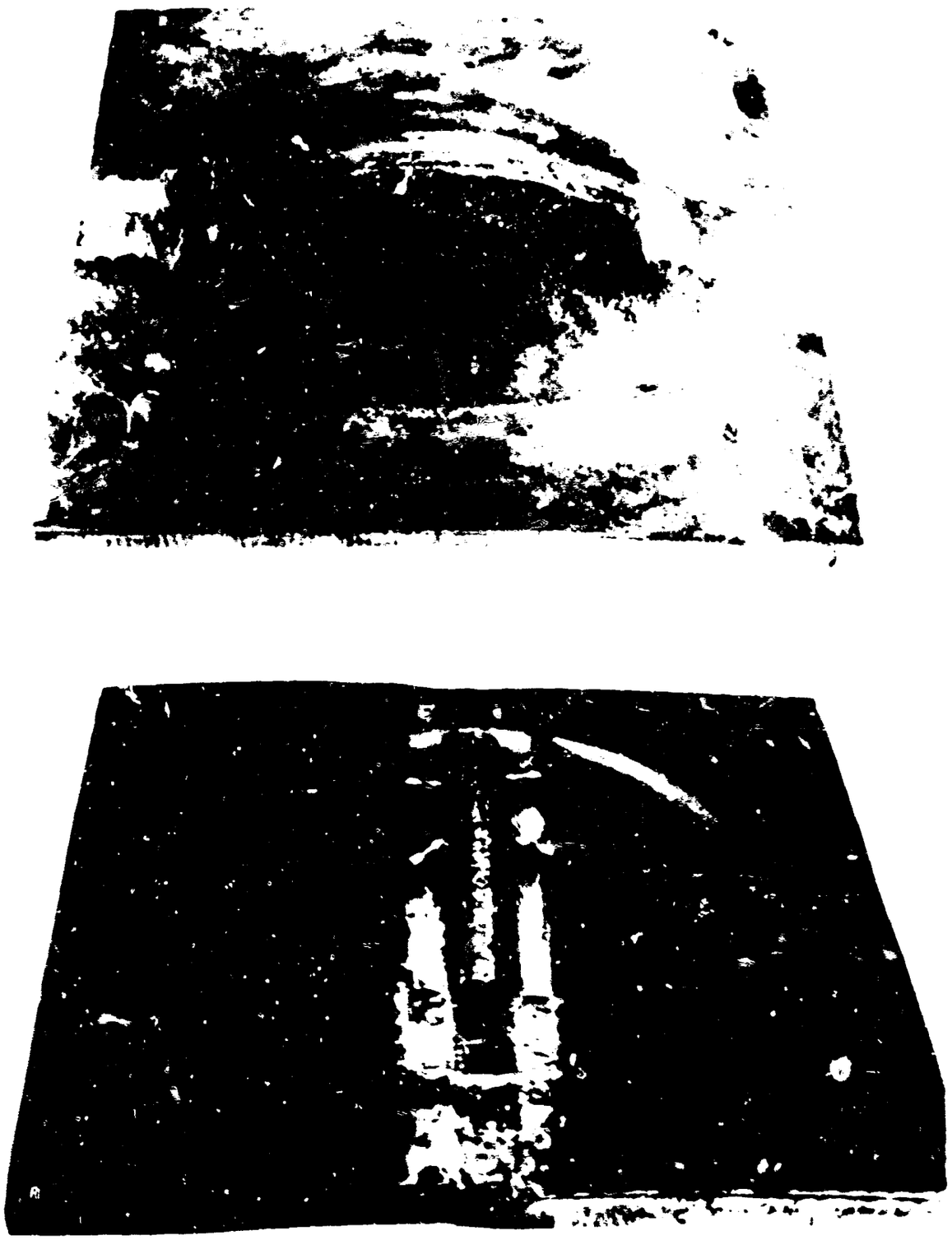

Fig. 13 - As-welded explosion bulge tests of 135 and 140-ksi yield strength MIG interrupted-arc (vertical-up) welds: upper, Airco plate after 4 shots; lower, Linde plate after 4 shots

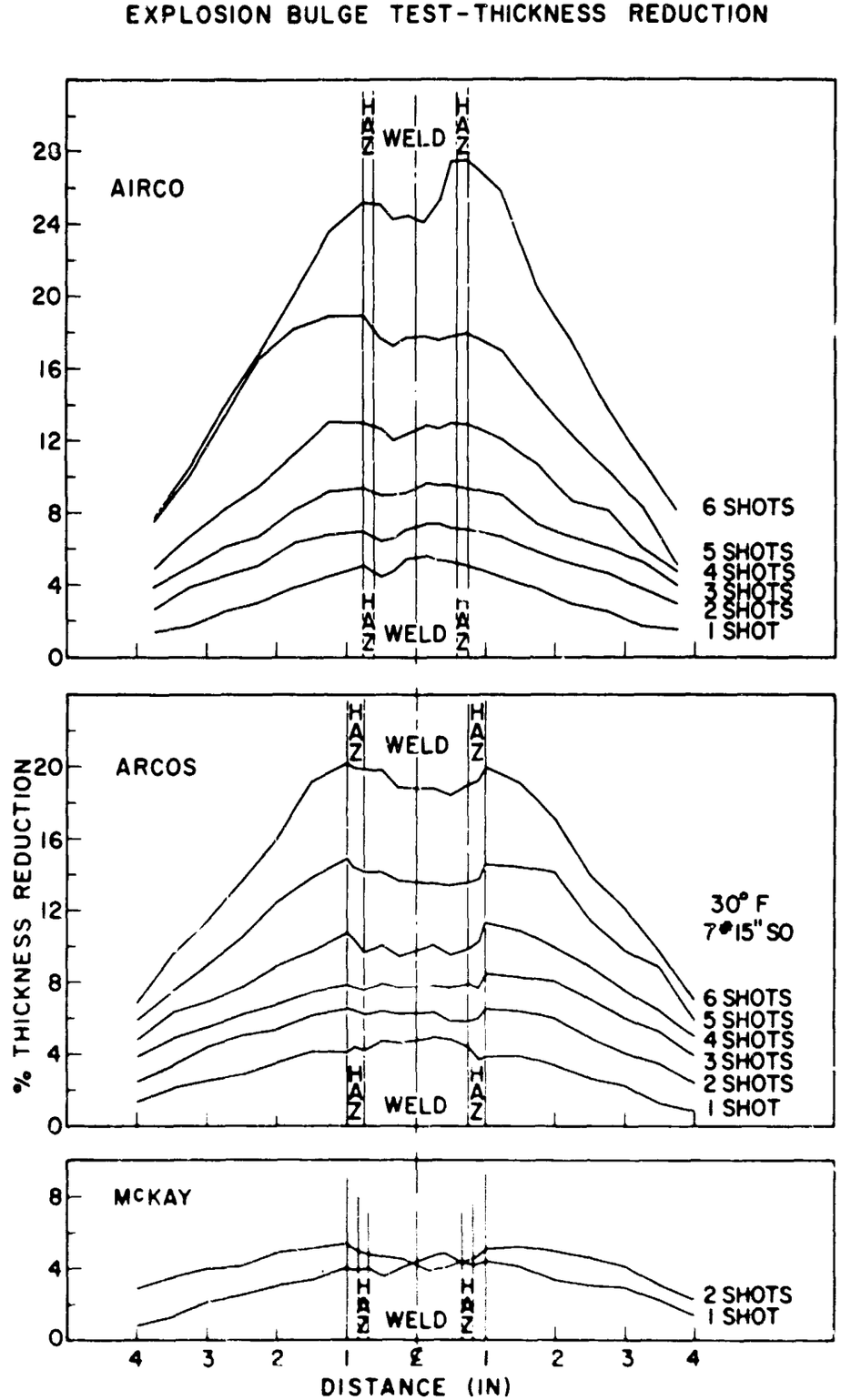

Fig. 14 - Plate and weld metal thickness reduction; explosion bulge testing of 140-ksi yield strength weld metals

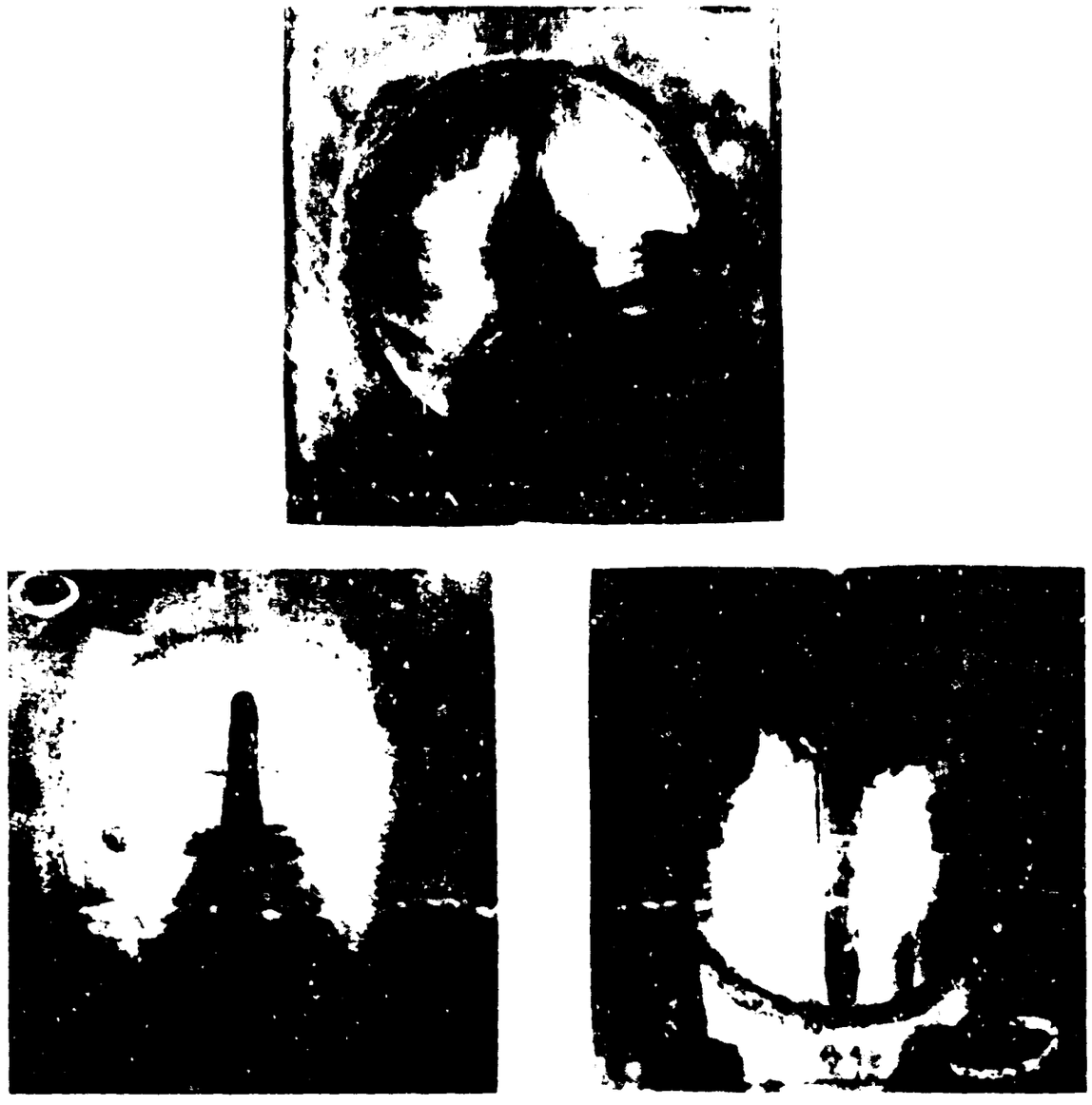

Fig. 15 - Weld crown ground-off explosion bulge tests of 140-ksi yield strength covered stick electrode welds: upper left, Airco plate after 6 shots; upper right, McKay plate after 2 shots: and lower, Arcos plate after 6 shots

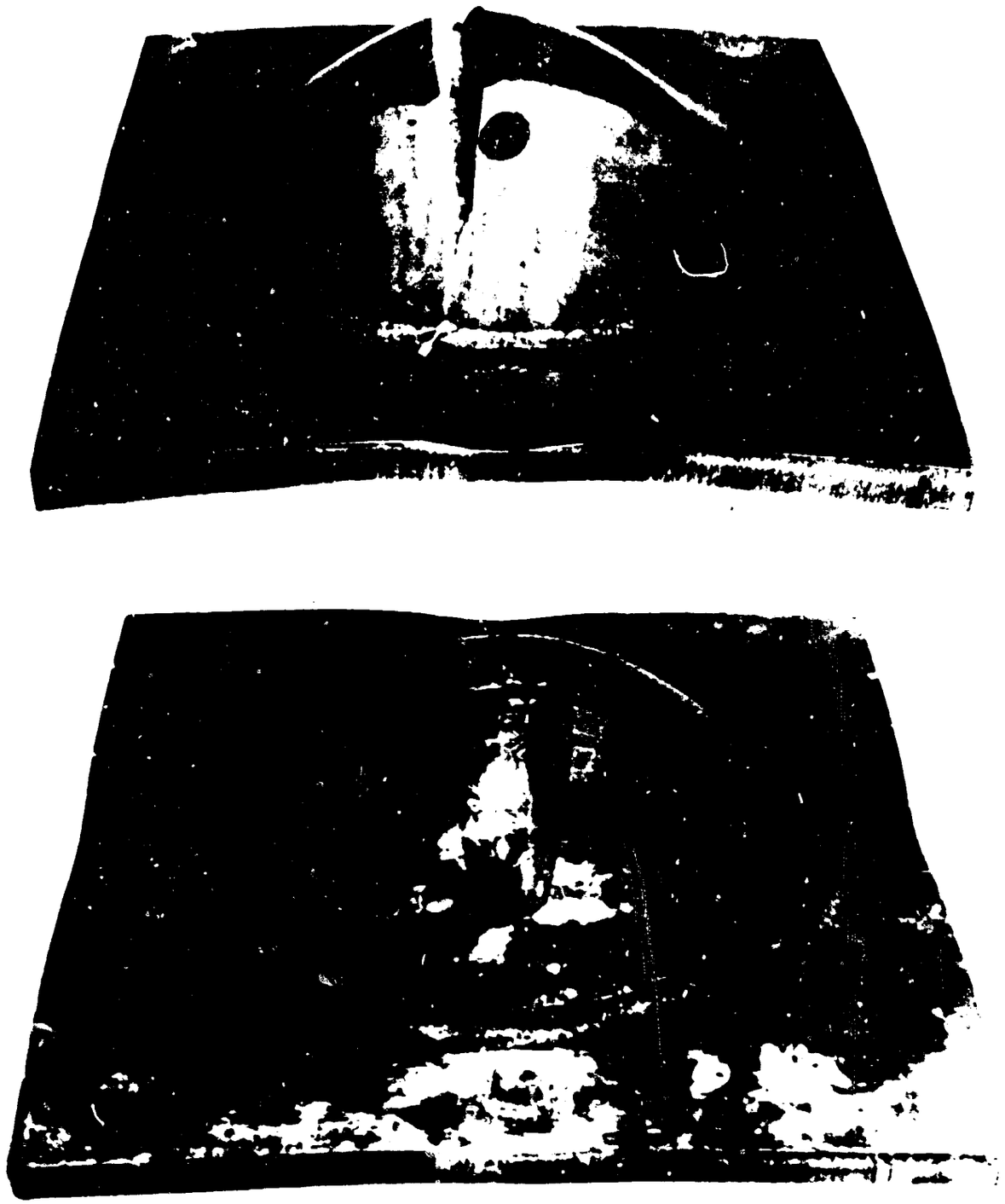

Fig. 16 - Weld crown ground-off explosion bulge tests of 135 and 140-ksi yield strength MIG interrupted-arc (vertical-up) welds: upper, Airco plate after 4 shots; lower, Linde plate after 6 shots

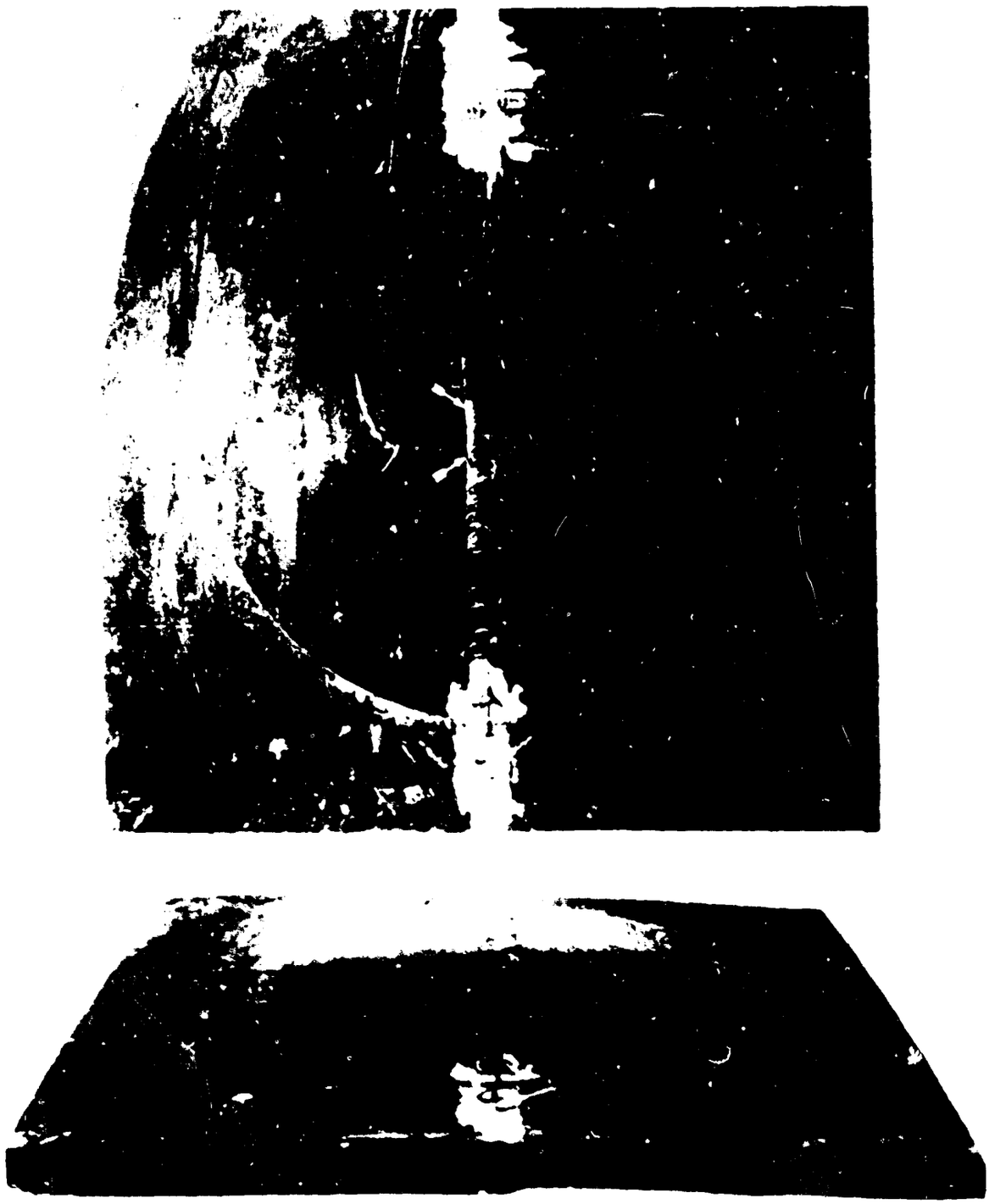

Fig. 17 - Explosion bulge test plate No. 1, 167-ksi yield strength TIG weld metal in 192-ksi yield strength 12-5-3 maraging steel: top, toe-crack after first 7-lb Pentolite shot; bottom, side view showing deformation

Fig. 18 - Plate of Fig. 17, after two 7-lb Pentolite shot; bottom, side view showing deformation

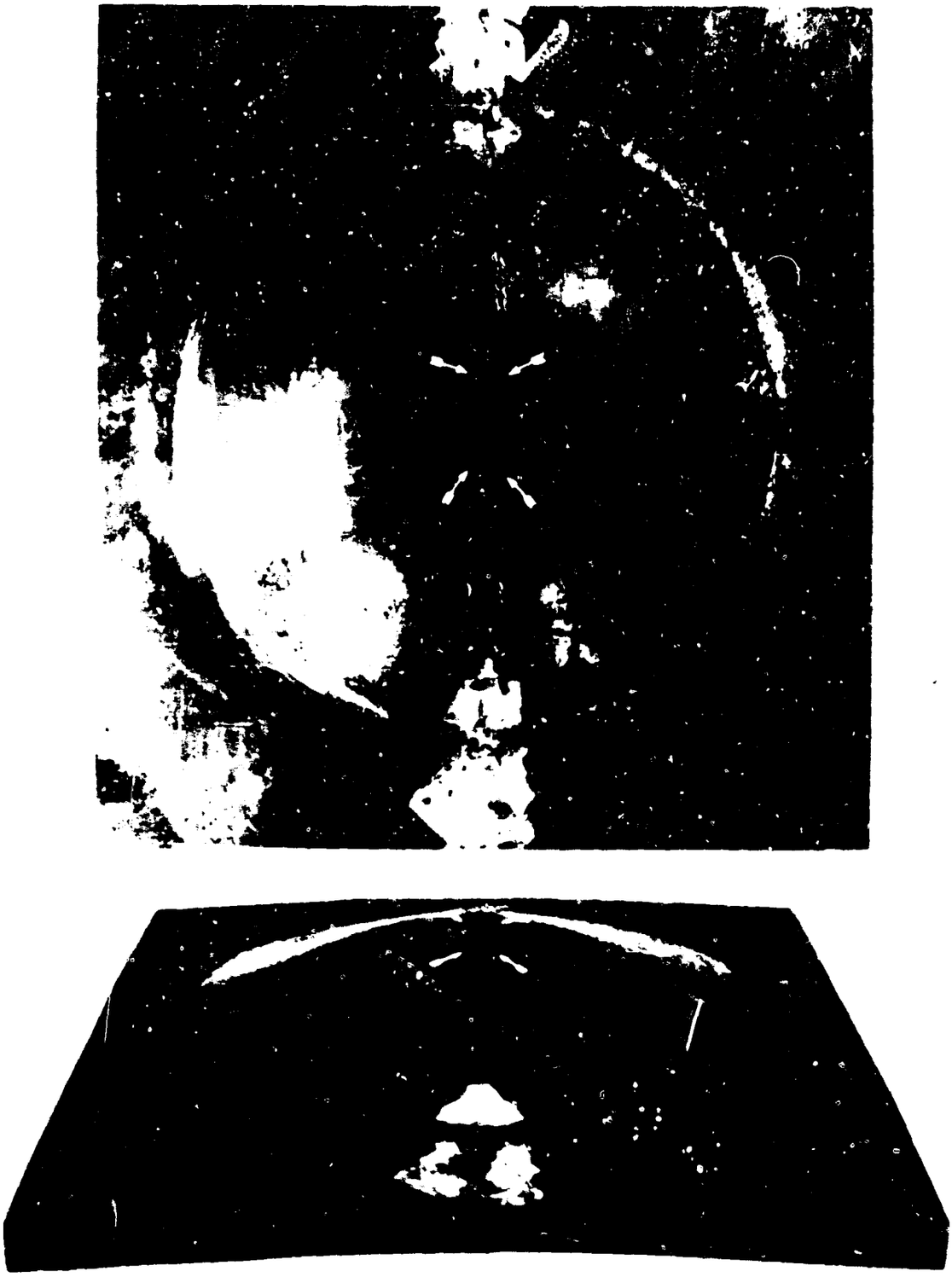

Fig. 19 - Explosion bulge test plate No. 2, matching TIG weld metal in 180-ksi yield strength 12-5-3 maraging steel: top, toe-cracks at edge of weld after three 7-lb Pentolite shots; bottom, side view showing deformation

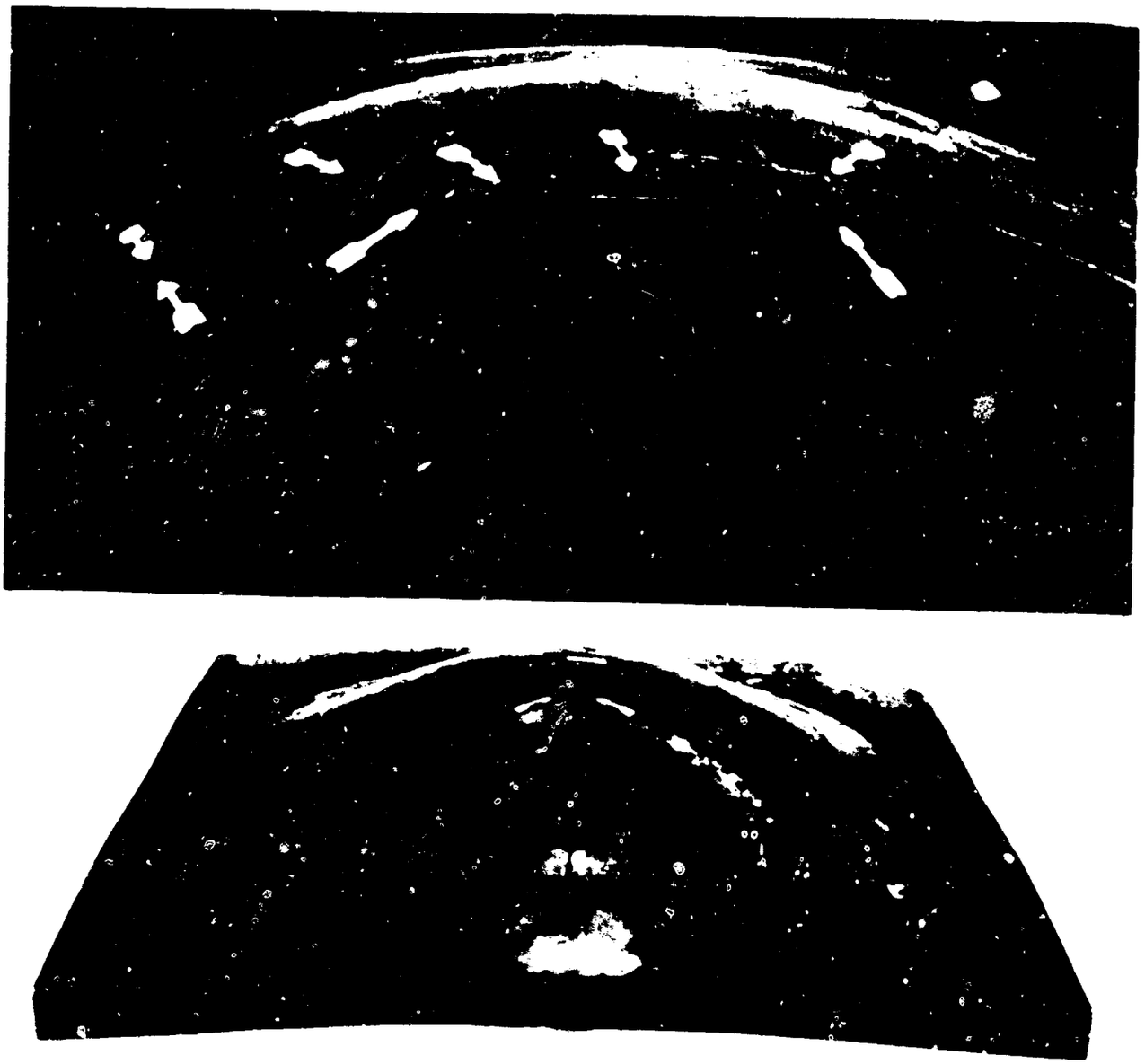

Fig. 20 - Plate of Fig. 19 after fourth 7-lb shot: top, enlarged view of weld cracks; bottom, side view of bulge

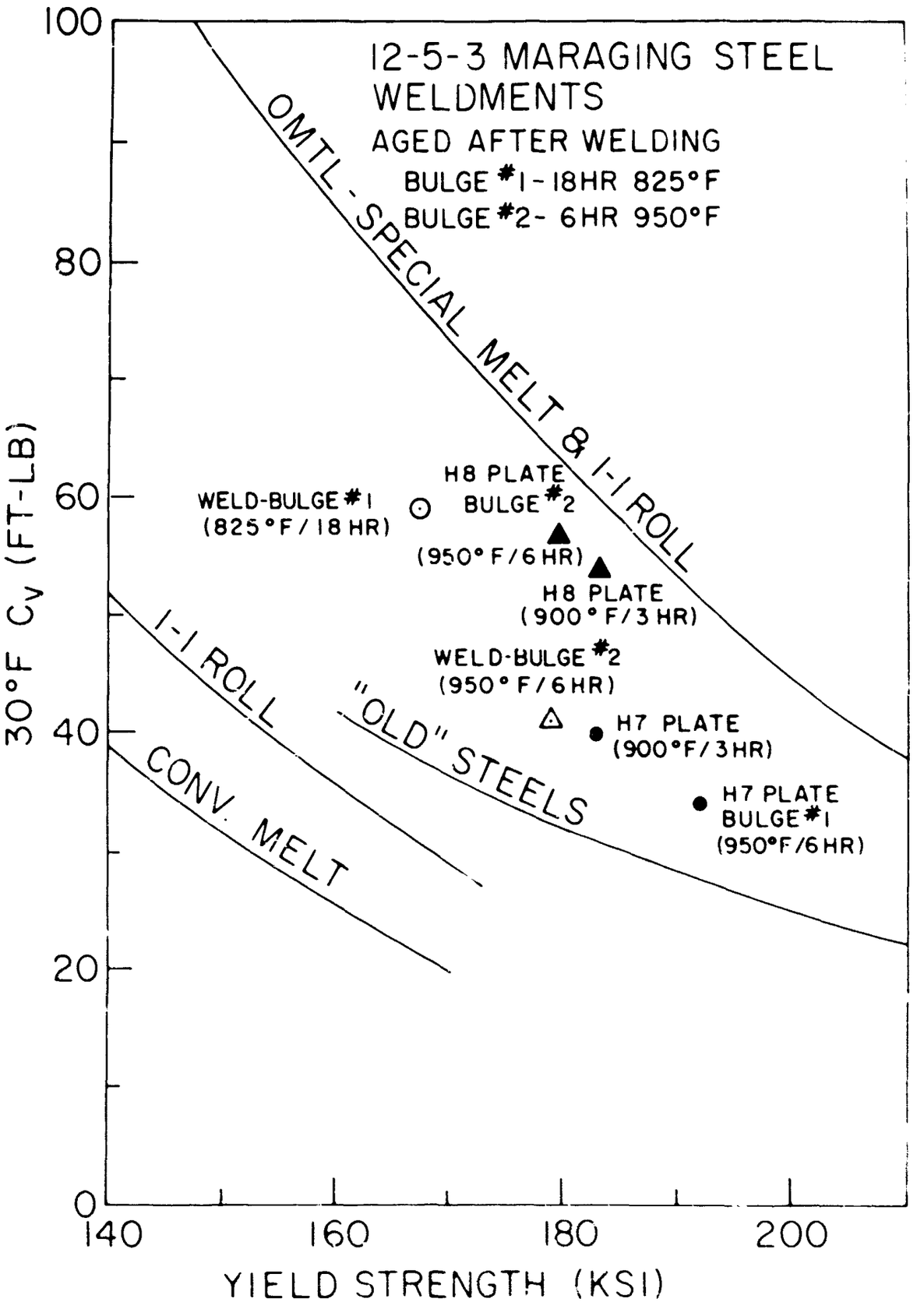

Fig. 21 - Charpy V energy as a function of yield strength for maraging steel plates and TIG weld metals in relation to previous data for 1-in.-thick plates

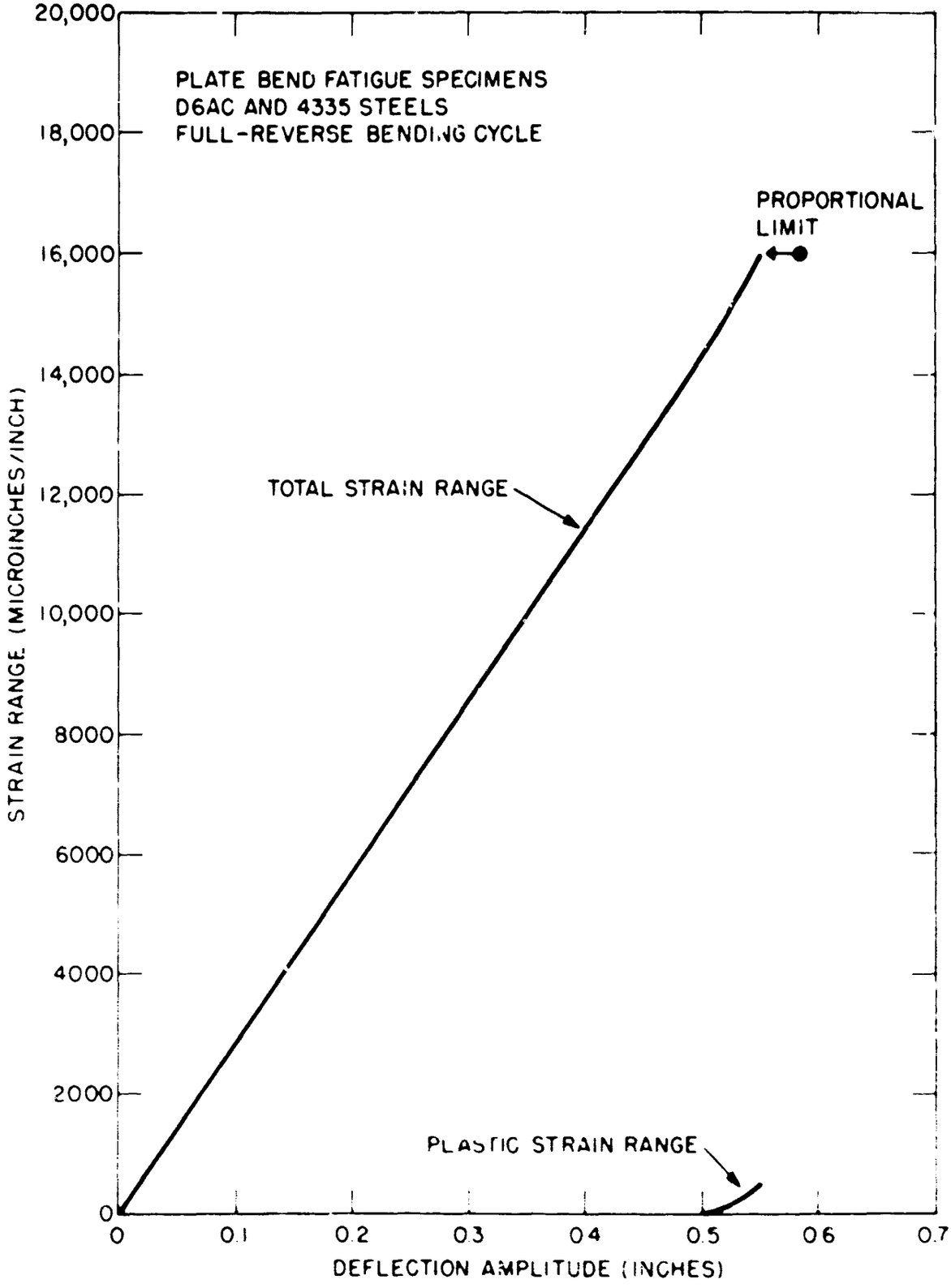

Fig. 22 - Strain range-deflection characteristics of D6AC and 4335 steel plate bend fatigue specimens in full-reverse loading cycle. The proportional limit point of 5000 microinches/inch plastic strain range is nearly identical for both materials.

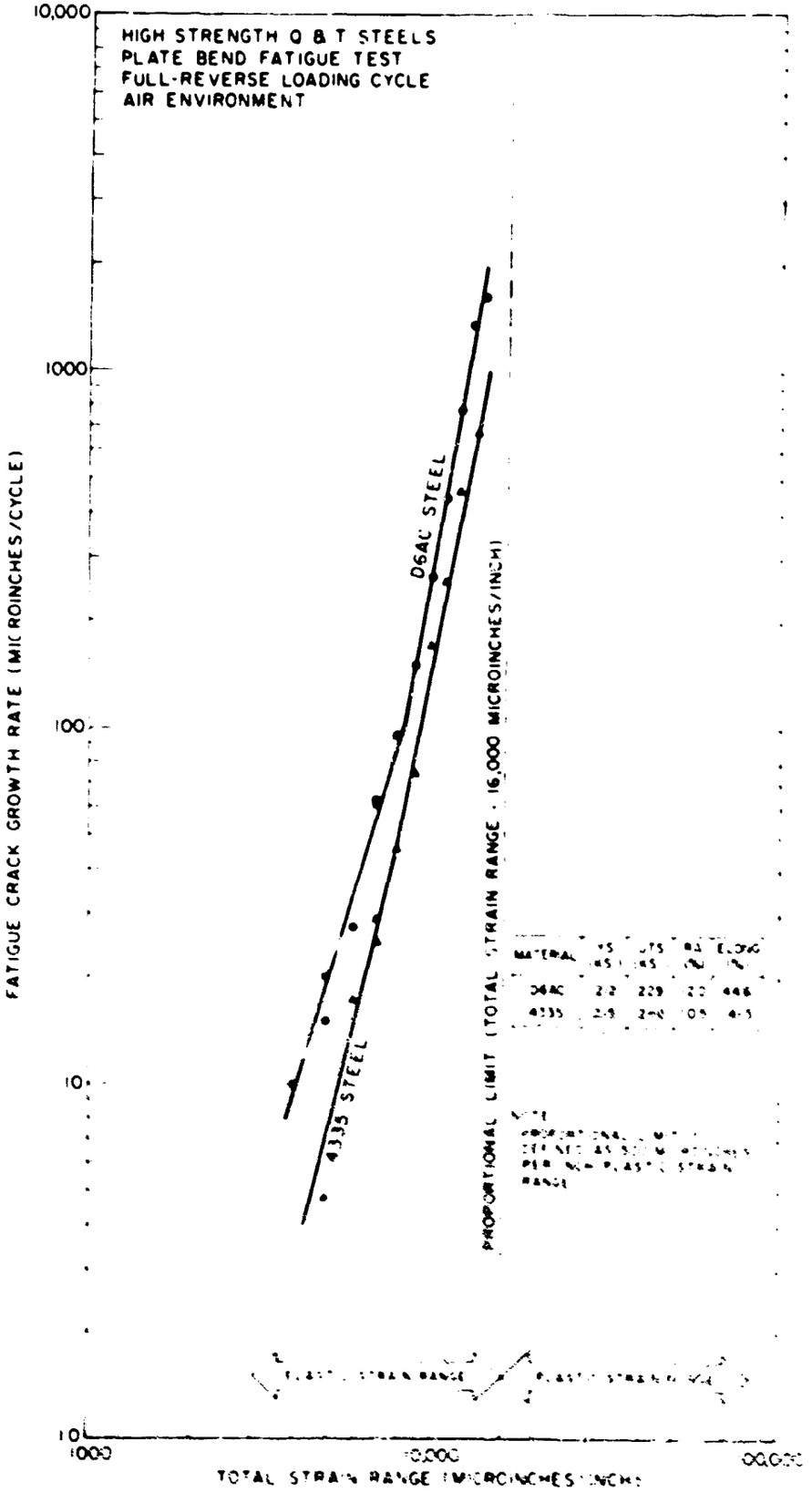

Fig. 23 - Log-log plot of fatigue crack growth rate vs applied total strain range data in full-reverse bending for D6AC and 4335 steels in an air environment

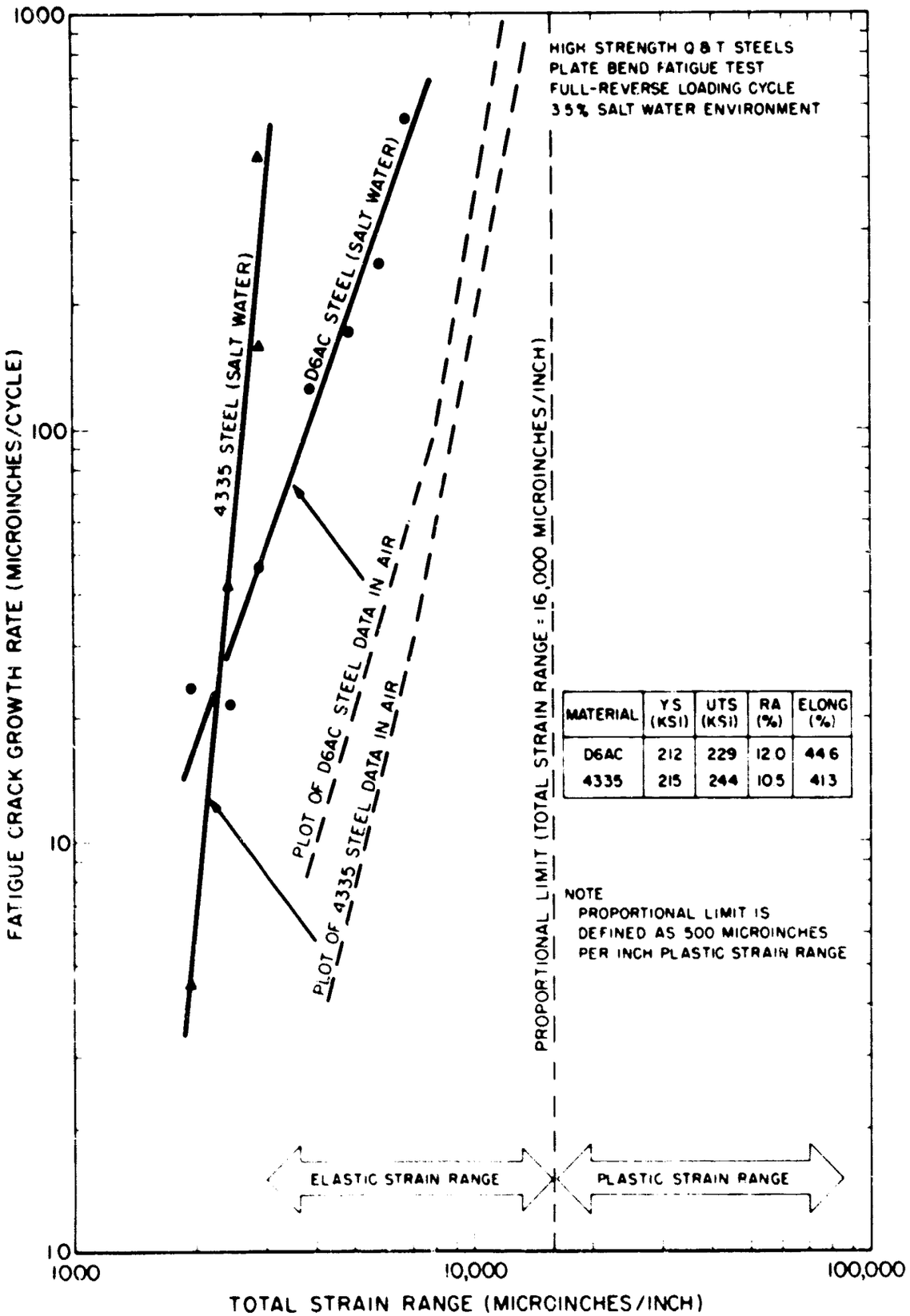

Fig. 24 - Log-log plot of fatigue crack growth rate vs applied total strain range data in full-reverse bending for D6AC and 4335 steels in 3.5% salt water environment. The loci of similar data obtained in an air environment are shown by dashed lines for comparison.

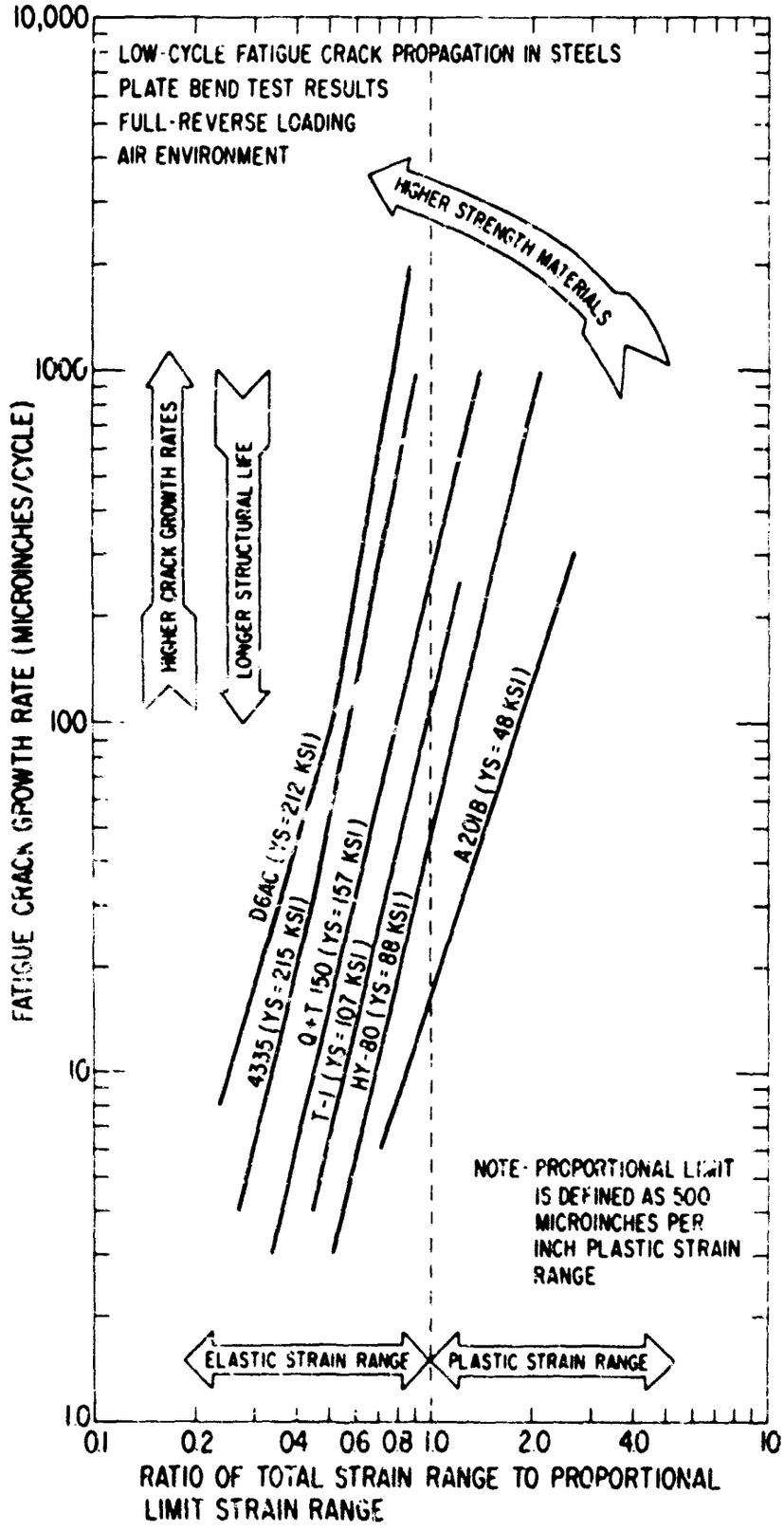

Fig. 25 - Comparative summary of the low cycle fatigue performance of six popular structural steels. Log-log plot shows fatigue crack growth rate vs the ratio of applied total strain range to proportional limit strain range.

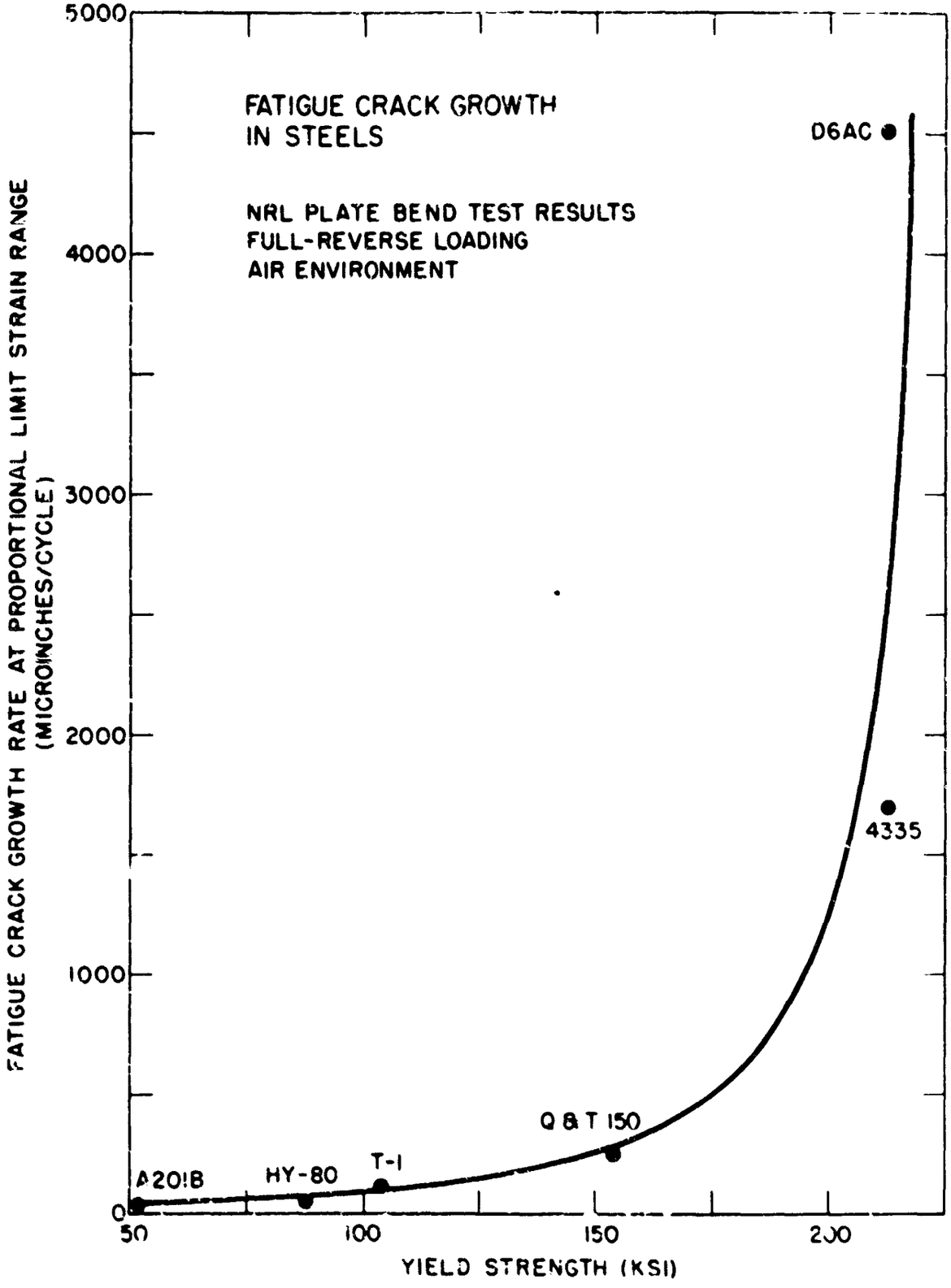

Fig. 26 - Comparison of fatigue crack growth rates at proportional limit strain range vs yield strength level for six popular structural steels

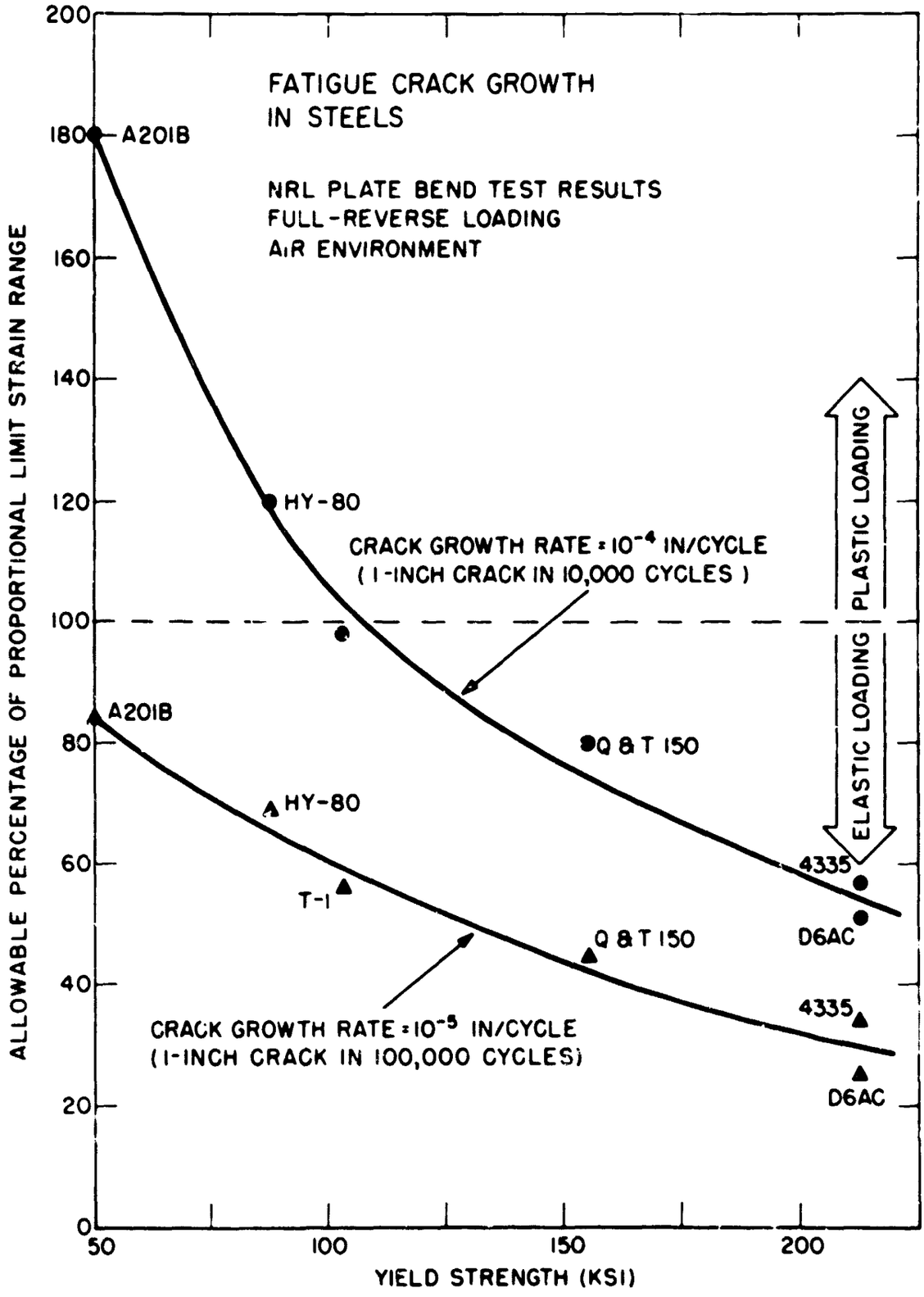

Fig. 27 - Comparison of allowable percentage of proportional limit strain range for finite fatigue life (10,000 and 100,000 cycles) vs yield strength level for six popular structural steels

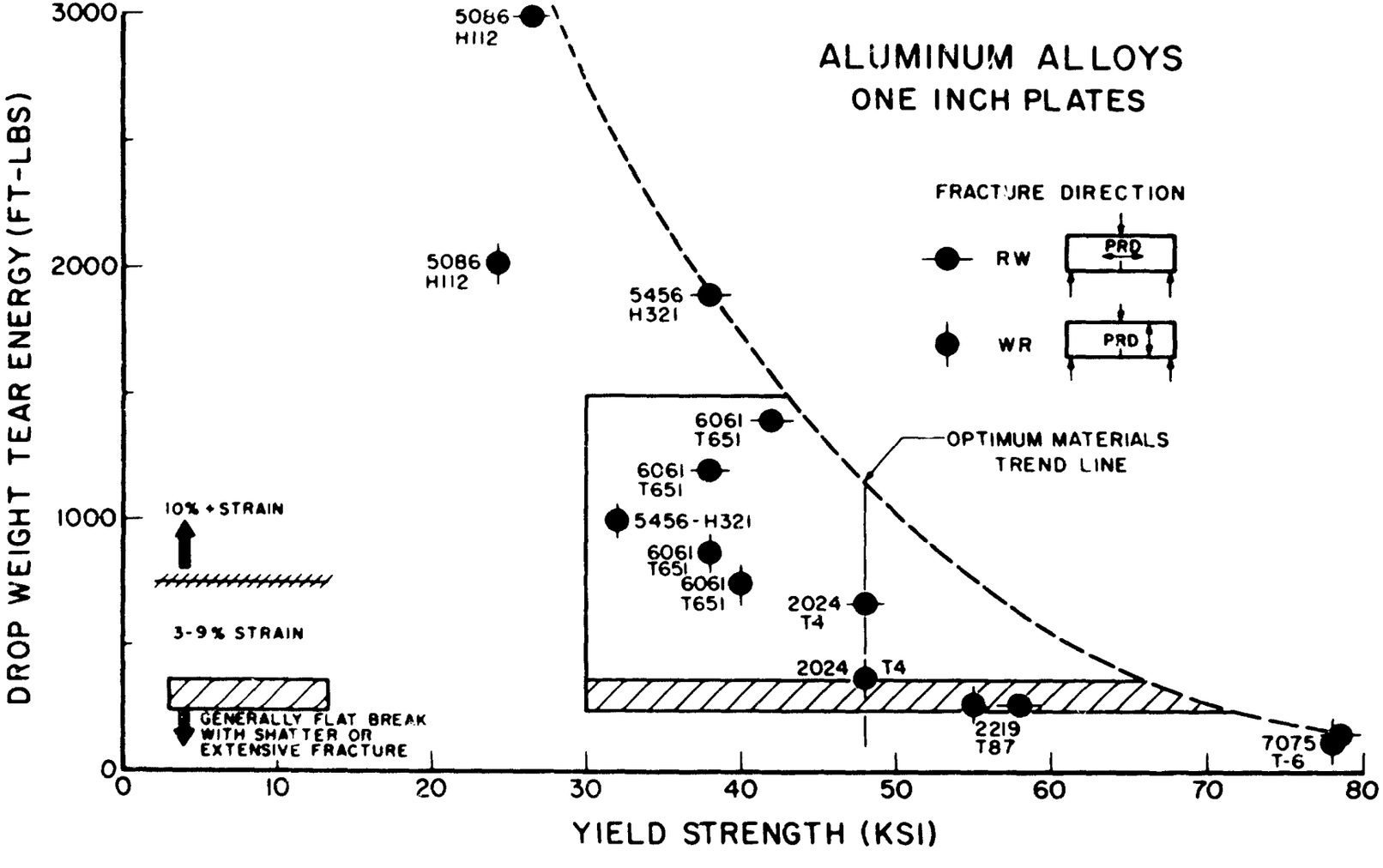

Fig. 28 - Fracture toughness index diagram (FTID) for aluminum alloys

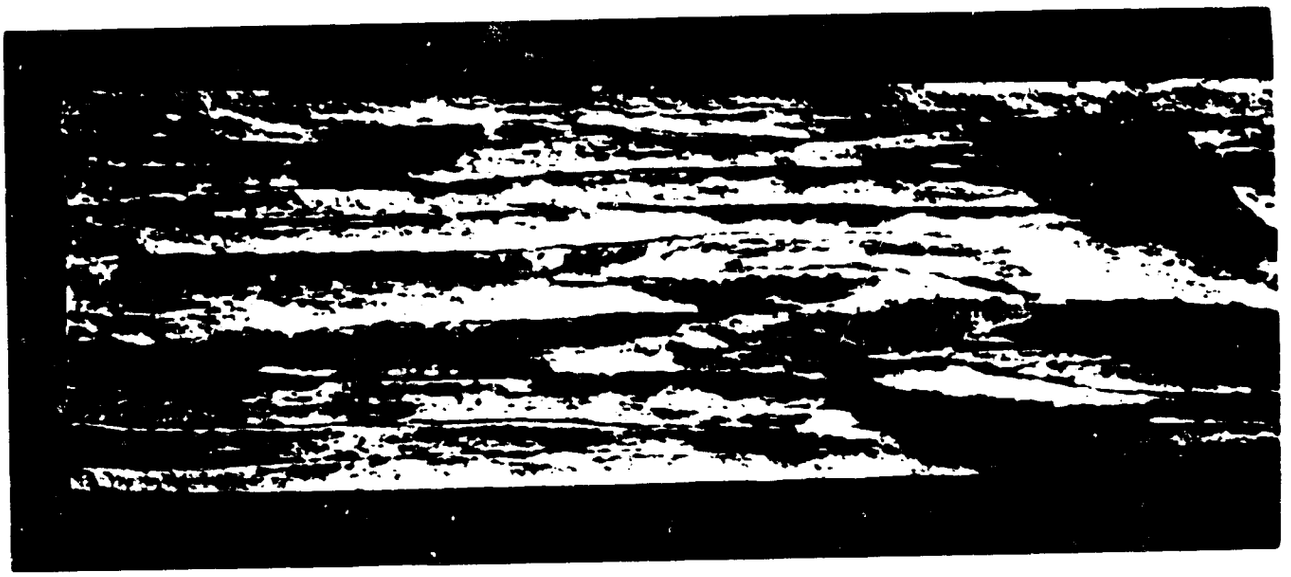

RW fracture direction

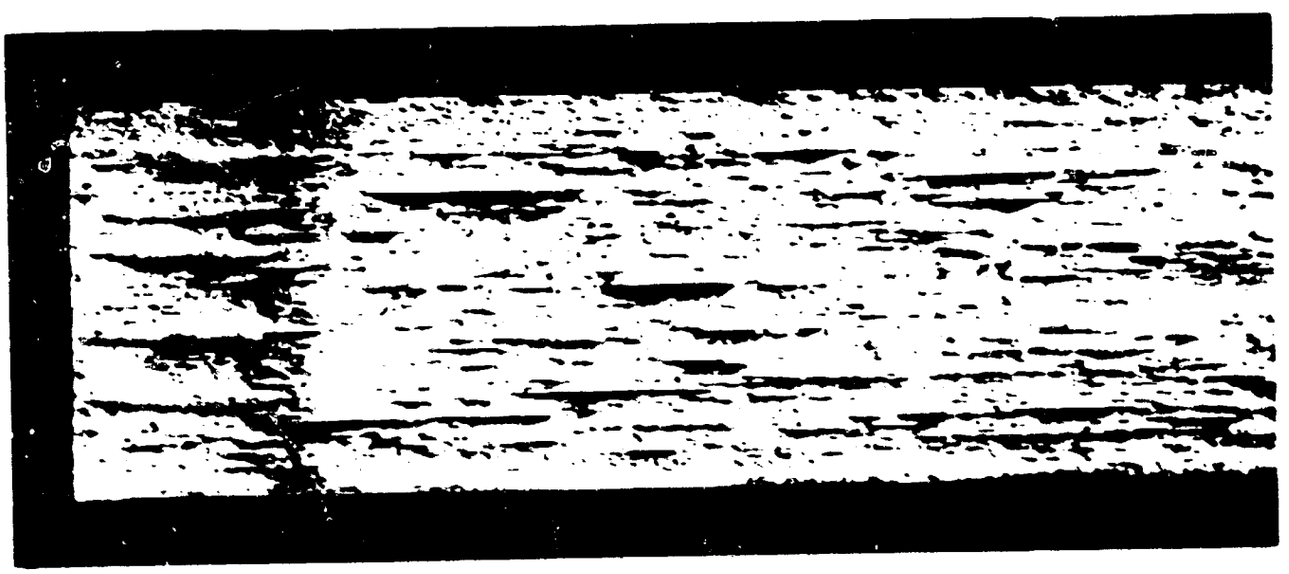

WR fracture direction

Fig. 29 - Fracture surfaces of 7079-T6 drop-weight tear test specimens showing apparent delamination

Fig. 30 - Explosion tear plate of 6061-T651 tested twice at 7.3% plastic strain. Fracture ran out at one end of plate. Flaw for the second test was 10-in. crack developed in first test.

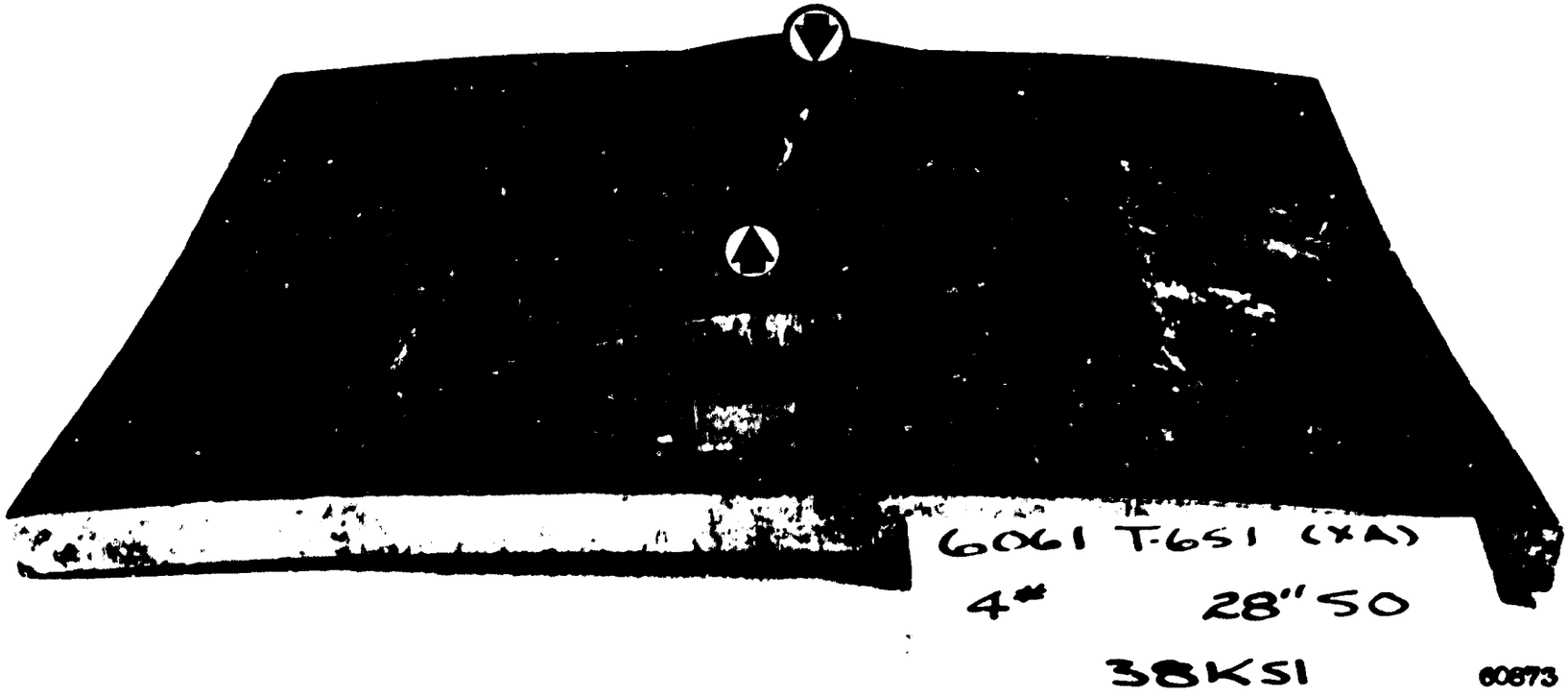

Fig. 31 - Explosion tear plate of 6061-T651 loaded to 8.2% plastic strain. Fracture extension approximately 11-inches.

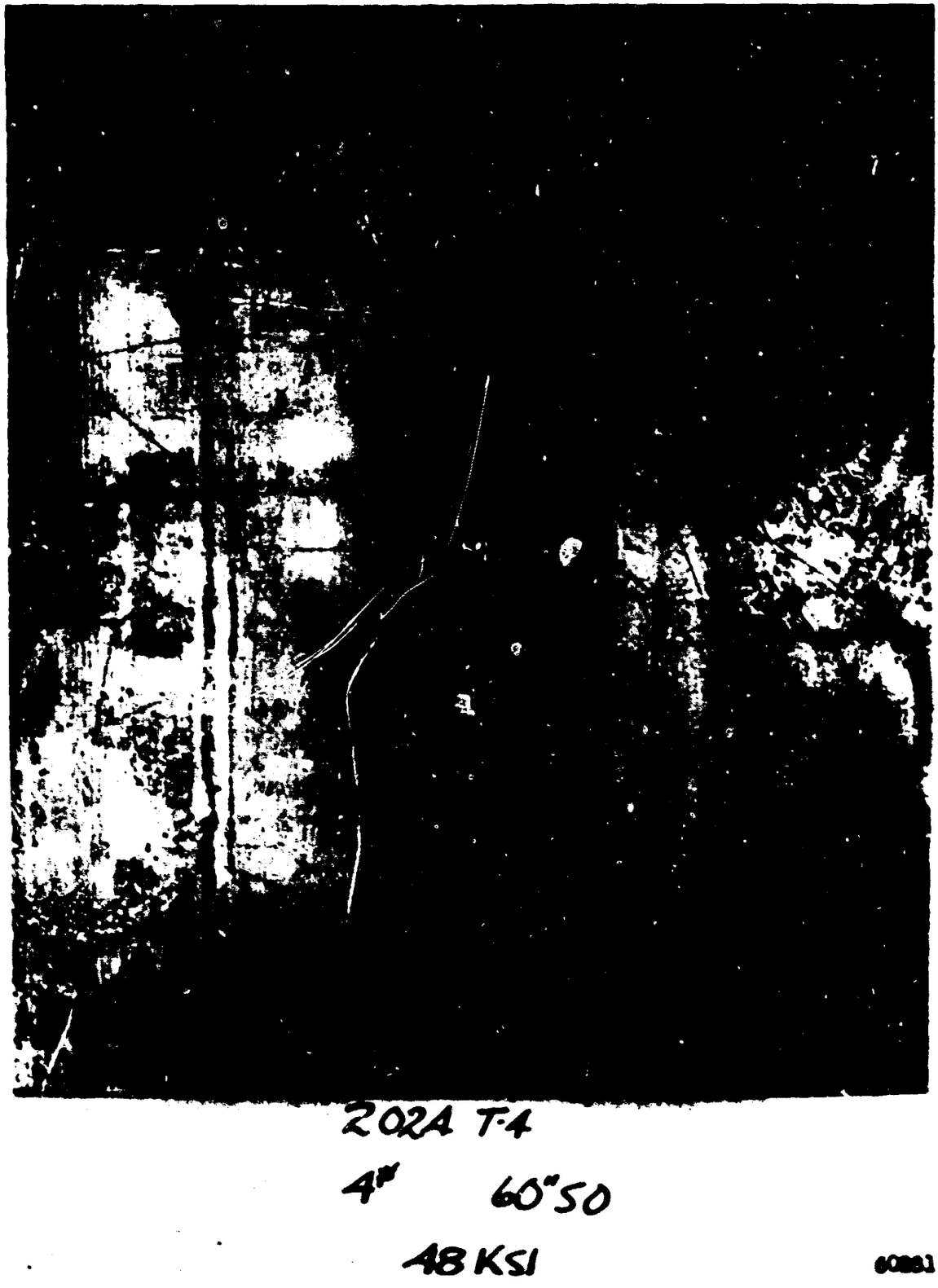

Fig. 32 - Explosion tear plate of 2024-T4 loaded to 3.7% plastic strain

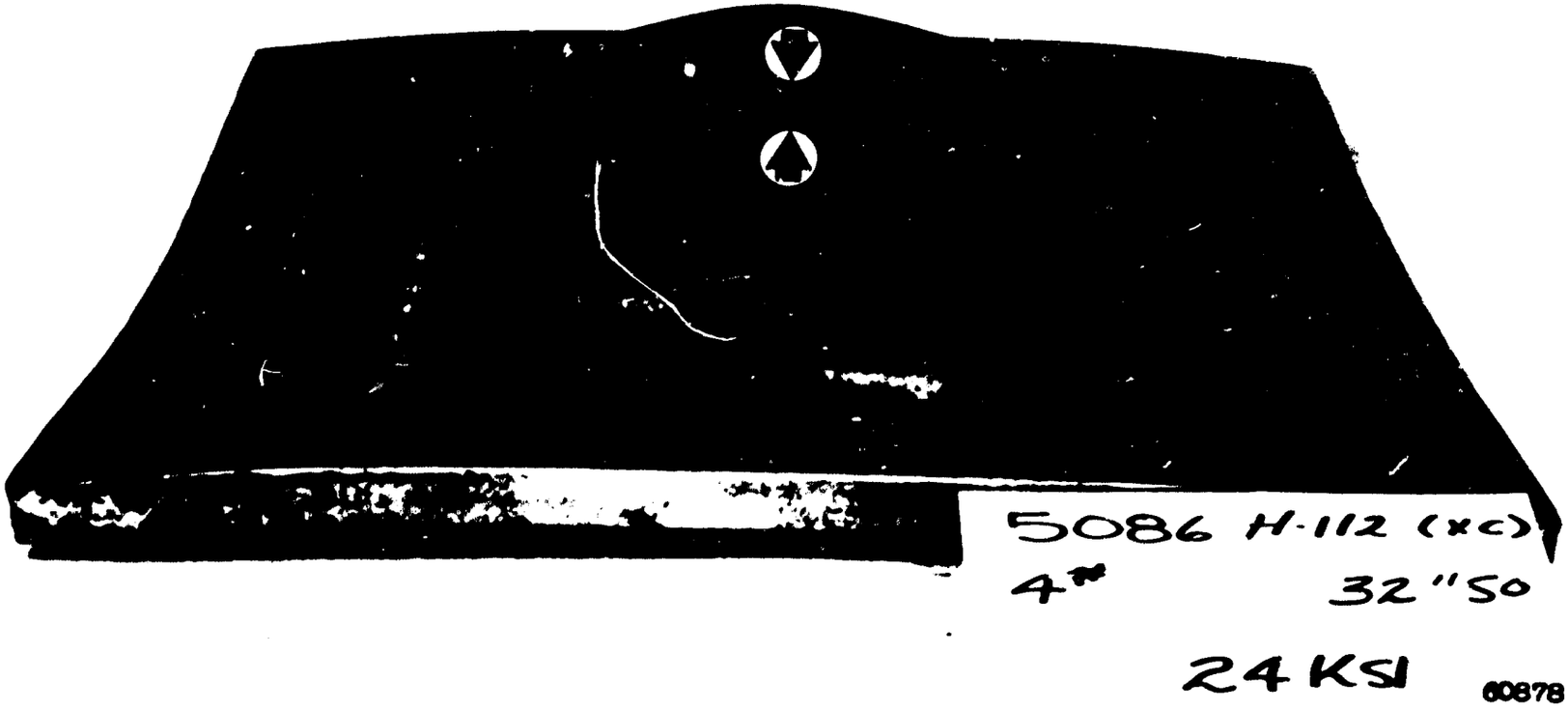

Fig. 33 - Explosion tear plate of 5086-H112 loaded to 8.3% plastic strain. Extent of fracture is shown by arrows.

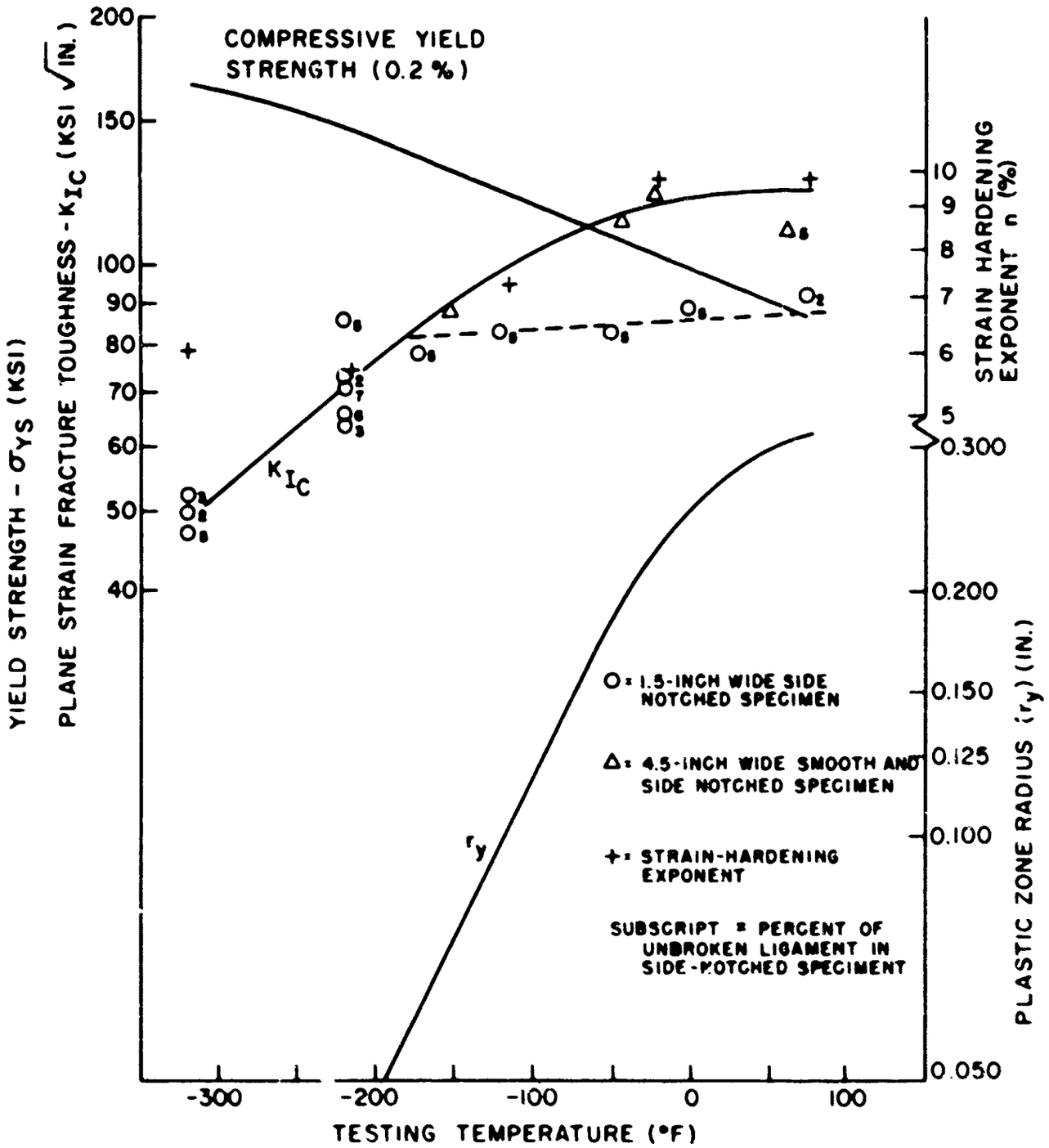

Fig. 34 - Correlation of K_{I_c} with testing temperature for 1.5-in. and 4.5-in.-wide specimens of unalloyed titanium

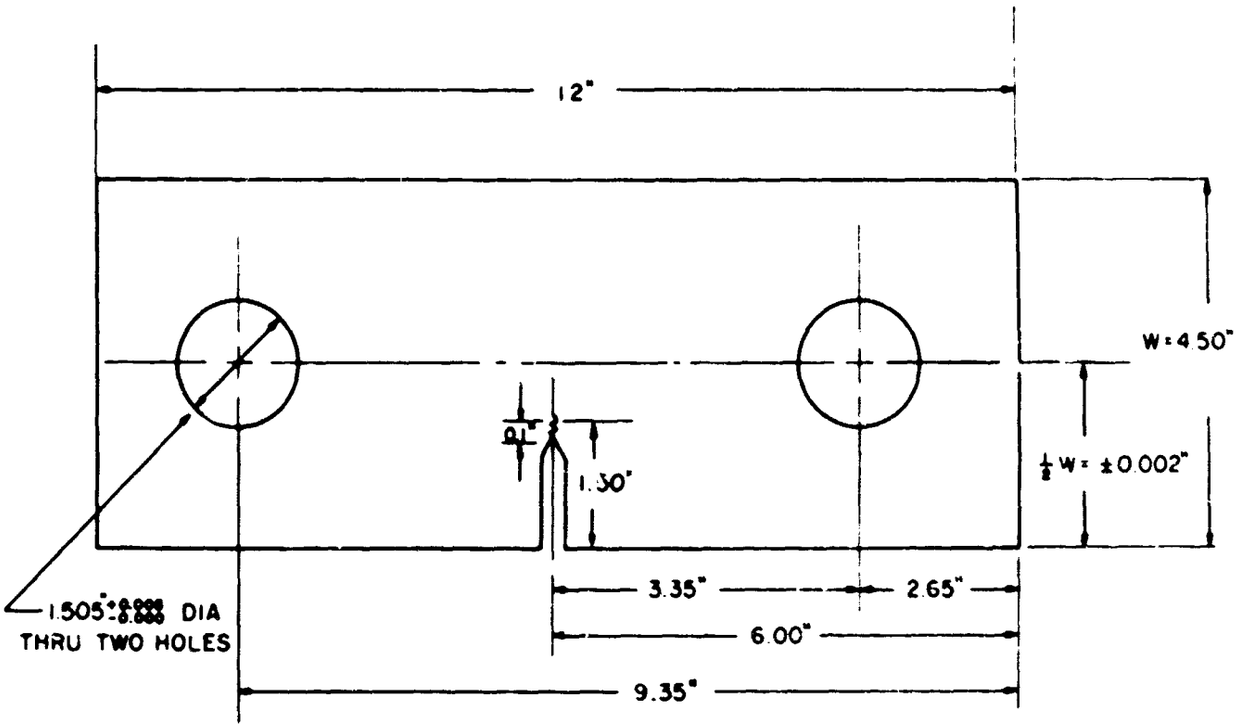

(a) FULL THICKNESS 1-INCH EDGE NOTCHED SPECIMEN

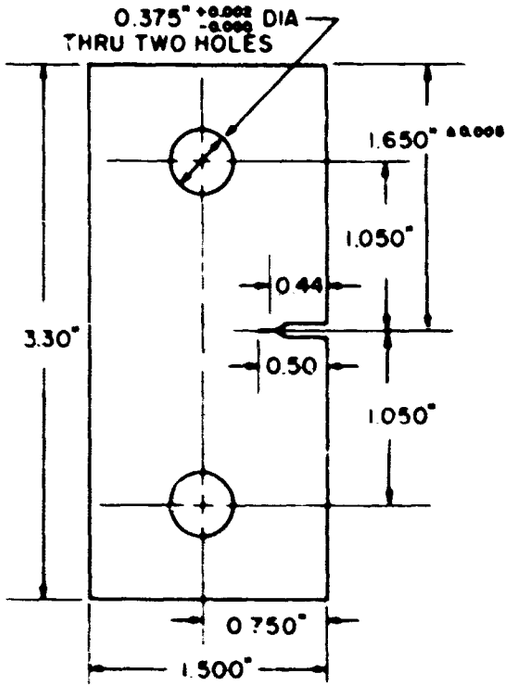

(b) QUARTER-INCH THICK EDGE NOTCHED SPECIMEN

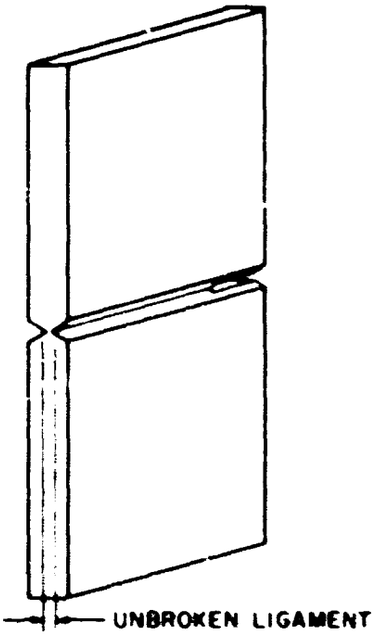

(c) SIDE-NOTCHED SPECIMEN

Fig. 35 - Dimension of specimens used in this report

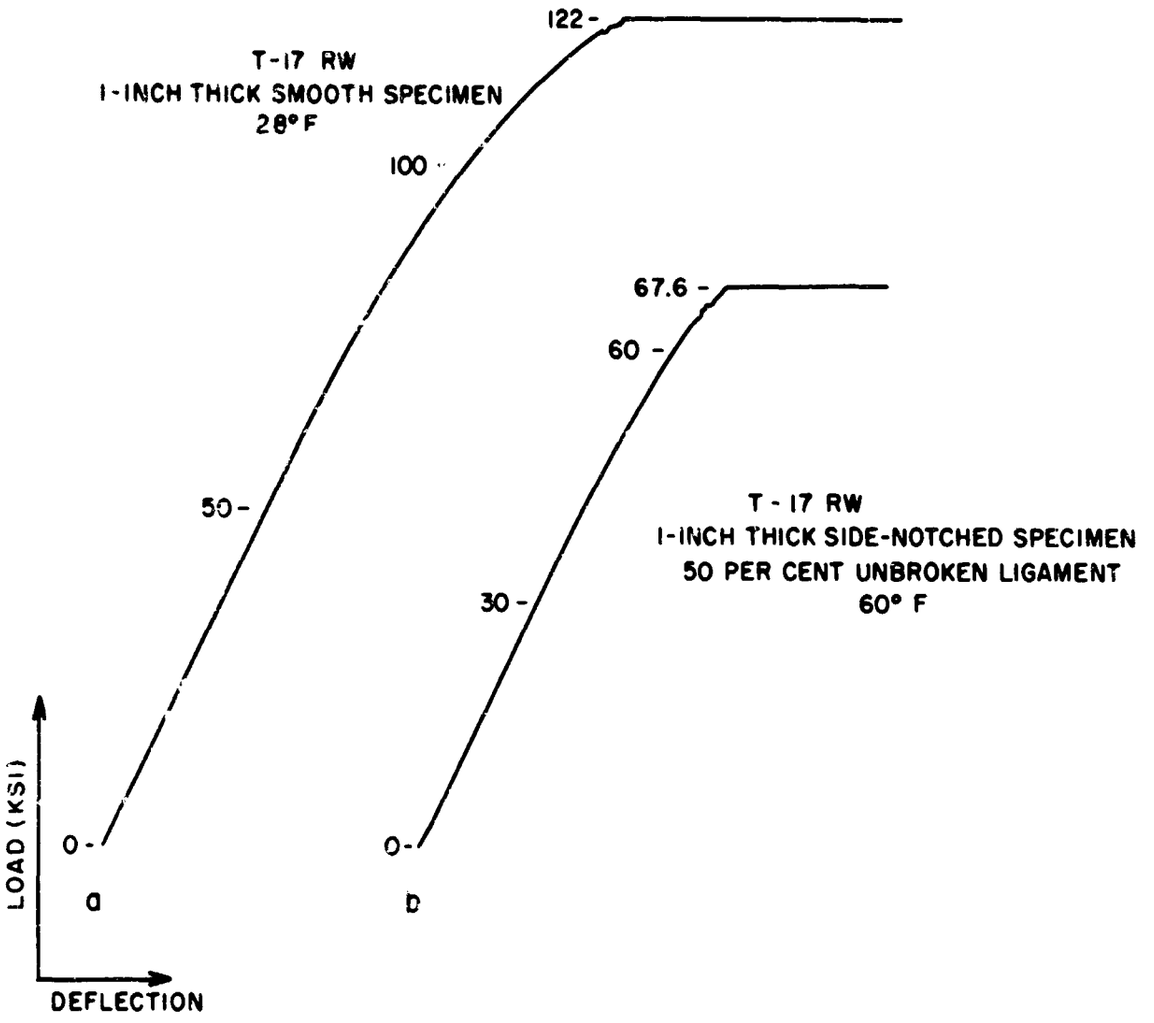

Fig. 36 - Typical load-deflection curves for smooth and side-grooved single-edge-notched specimens

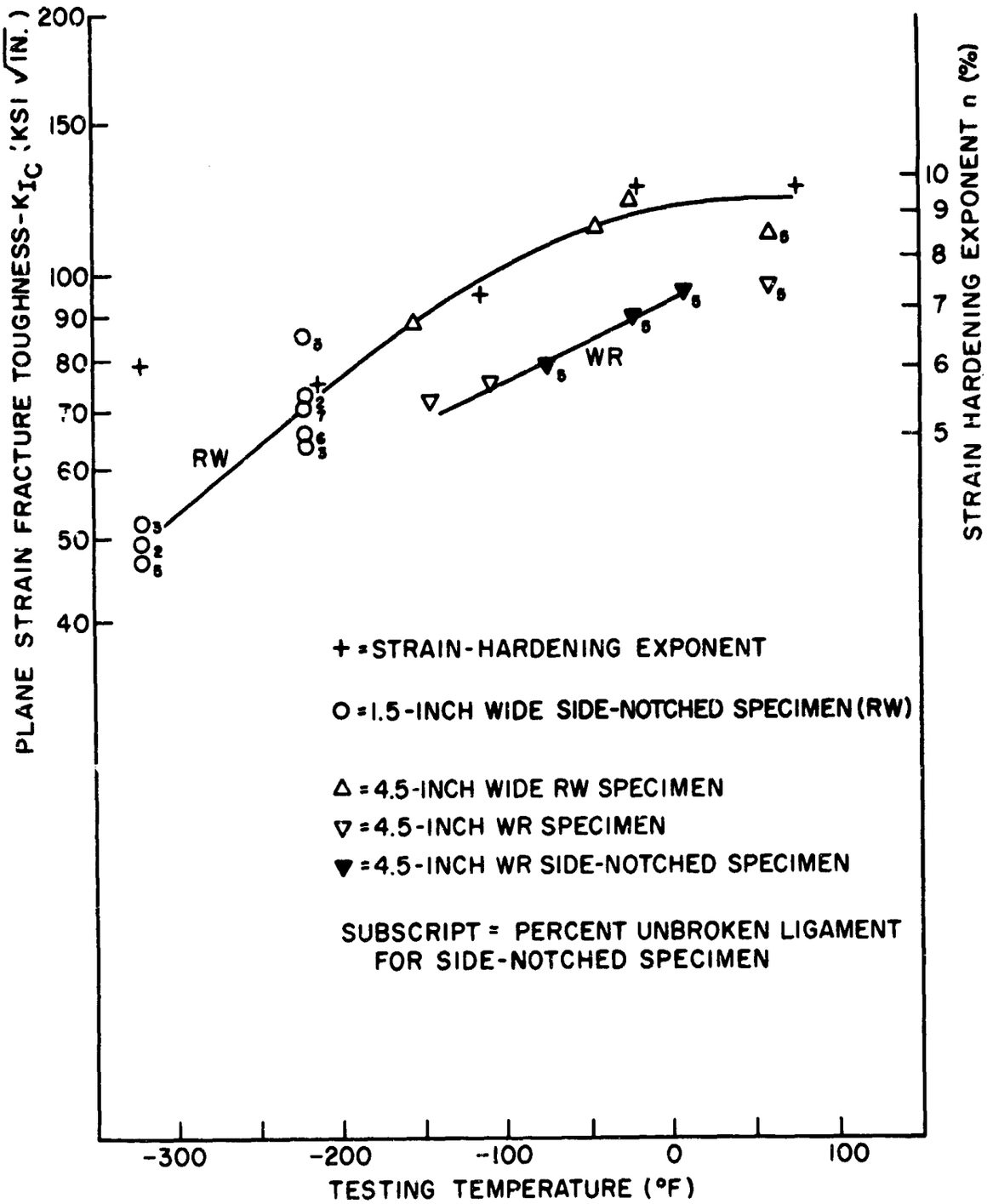

Fig. 37 - Correlation of K_{I_C} with test temperature for unalloyed titanium tested in the RW and WR directions